Acta Pharmaceutica Sinica B 2023;13(4):1631−1647

Chinese Pharmaceutical Association
Institute of Materia Medica, Chinese Academy of Medical Sciences

Acta Pharmaceutica Sinica B

www.elsevier.com/locate/apsb
www.sciencedirect.com

ORIGINAL ARTICLE

TRIB3 promotes pulmonary fibrosis through inhibiting SLUG degradation by physically interacting with MDM2

Xiaoxi Lv[a,*,†], Shanshan Liu[b,†], Chang Liu[c], Yunxuan Li[d], Tingting Zhang[d], Jie Qi[e], Ke Li[d], Fang Hua[a], Bing Cui[a], Xiaowei Zhang[a], Yuxin Liu[a], Jiaojiao Yu[a], Jinmei Yu[a], Li Li[a], Xia Li[e], Zhigang Yao[f], Bo Huang[g]

[a]*State Key Laboratory of Bioactive Substance and Function of Natural Medicines, Institute of Materia Medica, Chinese Academy of Medical Sciences & Peking Union Medical College, Beijing 100050, China*
[b]*National Clinical Research Center for Metabolic Diseases, Key Laboratory of Diabetes Immunology, Ministry of Education, And Department of Metabolism and Endocrinology, The Second Xiangya Hospital of Central South University, Changsha 410011, China*
[c]*Drug Clinical Trial Institution, Children's Hospital, Capital Institute of Pediatrics, Beijing 100020, China*
[d]*Institute of Medicinal Biotechnology, Chinese Academy of Medical Sciences & Peking Union Medical College, Beijing 100050, China*
[e]*Shandong University, Weihai 264209, China*
[f]*Department of Respiratory Medicine, Beijing Friendship Hospital, Capital Medical University, Beijing 100050, China*
[g]*Institute of Basic Medicine, Chinese Academy of Medical Sciences & Peking Union Medical College, Beijing 100005, China*

Received 10 January 2022; received in revised form 9 November 2022; accepted 11 November 2022

KEY WORDS

E3 ligase;
Lung injury;
MDM2;
Protein−protein interaction;

Abstract Pulmonary fibrosis (PF) is the pathological structure of incurable fibroproliferative lung diseases that are attributed to the repeated lung injury-caused failure of lung alveolar regeneration (LAR). Here, we report that repetitive lung damage results in a progressive accumulation of the transcriptional repressor SLUG in alveolar epithelial type II cells (AEC2s). The abnormal increased SLUG inhibits AEC2s from self-renewal and differentiation into alveolar epithelial type I cells (AEC1s). We found that the elevated SLUG represses the expression of the phosphate transporter SLC34A2 in AEC2s, which

*Corresponding author. Tel./fax: +86 10 83165034.
E-mail address: lvxiaoxi@imm.ac.cn (Xiaoxi Lv).
†These authors made equal contributions to this work.
Peer review under responsibility of Chinese Pharmaceutical Association and Institute of Materia Medica, Chinese Academy of Medical Sciences.

https://doi.org/10.1016/j.apsb.2023.01.008

Proteolysis;
Ubiquitination;
UPS

reduces intracellular phosphate and represses the phosphorylation of JNK and P38 MAPK, two critical kinases supporting LAR, leading to LAR failure. TRIB3, a stress sensor, interacts with the E3 ligase MDM2 to suppress SLUG degradation in AEC2s by impeding MDM2-catalyzed SLUG ubiquitination. Targeting SLUG degradation by disturbing the TRIB3/MDM2 interaction using a new synthetic staple peptide restores LAR capacity and exhibits potent therapeutic efficacy against experimental PF. Our study reveals a mechanism of the TRIB3−MDM2−SLUG−SLC34A2 axis causing the LAR failure in PF, which confers a potential strategy for treating patients with fibroproliferative lung diseases.

1. Introduction

Pulmonary fibrosis (PF) is not only considered an independent alveolar lung disease but is also recognized as the crucial pathological change in a range of chronic fibroproliferative lung diseases[1]. Although advanced IPF patients can be treated with lung transplantation, only a few patients receive this therapy due to limited donor organ resources[2]. Recent studies have not only provided significant mechanistic insight into PF pathogenesis but also have two FDA-approved anti-PF agents with definite promise[3,4], although neither of them have been shown to confer a significant survival benefit in clinical trials[2]. Thus, new, safer and more effective anti-PF drugs are urgently needed.

There are distinct differences between acute and chronic lung injury induced PF. Patients who are infected with coronavirus (COVID-19) may develop to respiratory failure derived from acute respiratory distress syndrome (ARDS), and a considerable percentage of the survivors of COVID-19 ARDS progress to PF[5]. However, the post-ARDS PF is not progressive and recoverable[6]. The recovery period for the post-ARDS PF takes one year, indicating that the lung regeneration occurs in acute lung injury induced PF. However, persistent and repeated injury to the lung epithelium causes chronic inflammation and irreversible PF, suggesting that failure of lung alveolar regeneration (LAR) is an important mechanism in progressive PF[7,8]. Although several types of cells are involved in lung regeneration[9], alveolar epithelial type 2 cells (AEC2s), which have secretory, host defense, self-renewal and differentiation [into alveolar epithelial type 1 cells (AEC1s)] abilities, are the main alveolar stem cells responsible for LAR[10]. AEC2s undergo rapid proliferation and differentiation in response to acute lung injury[11], but the epithelial cells sorted from IPF patients using AEC2 markers present a diversity of transcriptional states compared with cells sorted from healthy donors, suggesting AEC2 dysfunction in PF pathogenesis[12]. Additionally, the self-renewal and the differentiation capacity of AEC2s are limited in patients with IPF[13,14]. Although transplantation of pluripotent stem cell-derived AEC2s holds great promise for the treatment of diseases affecting lung alveoli[15,16], understanding the molecular mechanism of AEC2 dysfunction in PF may be a key for developing anti-PF drugs.

Recent studies have indicated that the transcription repressor SLUG is upregulated in alveolar epithelial cells from IPF patients, and the changed AEC2s trigger fibroblast activation *via* their secretory phenotype[12,17,18]. As a zinc-finger transcriptional repressor of the SNAIL superfamily, SLUG inhibits the transcription of a set of genes involved in adhesion, differentiation, stemness and cellular plasticity through sequence-specific interaction with DNA[19]. SLUG also promotes cancer development by controlling stem cell self-renewal and differentiation[20] and regulates epithelial cell survival and wound healing[21]. Furthermore, SLUG promotes the development of pulmonary hypertension secondary to PF through regulating the function of macrophage[22]. In this study, we hypothesized that elevated SLUG expression contributes to LAR failure by impeding AEC2 self-renewal and differentiation in PF. Therefore, we proposed that accelerating SLUG degradation might be a promising therapeutic strategy directed at LAR failure to reduce PF development and progression.

2. Materials and methods

2.1. Human fibrotic lung specimens

The human normal lung specimens surgically removed from autopsy tissue following accidental death and the human fibrotic lung specimens used for Western blotting and confocal analyses were obtained from Alenabio (Xi'an, China). Frozen sections of human normal and fibrotic lung tissues were purchased from OriGene Inc. (MD, USA). The frozen sample IDs are FR00016BFA, FR5B33585A, FR000180AD, FR5B33819D, FR5B336AFD, and FR0001809E. All protocols using human specimens were approved by the Institutional Review Board of the Chinese Academy of Medical Sciences and Peking Union Medical College. Informed consent was obtained from all subjects. The study conforms to the principles outlined in the Declaration of Helsinki.

2.2. Animal studies

B6; FVB-Tg (SFTPC-rtTA)5 Jaw Tg (tetO-cre)1 Jaw/Smoc (*Sftpc-TetO-Cre*) mice and B6.129X1-Gt (ROSA)26Sortm1 (EYFP)Cos/J (*ROSA-EYFP*) mice were purchased from Shanghai Model Organisms Center, Inc. B6.129S1-Snai2<tm1Grid>/J mice were purchased from Jackson Laboratories. *Sftpc-TetO-Cre* mice were crossed with ROSA-EYFP mice to generate *Sftpc-Cre;ROSA-EYFP* mice. *Sftpc-Cre;ROSA-EYFP* mice were maintained on water containing doxycycline (1 mg/mL) after the vehicle or BLM challenge. *Trib3* conditional knockout ($Trib3^{flox/flox}$) mice were generated as previously described[23]. *Sftpc-TetO-Cre* mice were crossed with $Trib3^{flox/flox}$ mice to generate *Sftpc-Cre;* $Trib3^{flox/flox}$ mice. C57 BL/6 mice (18 g, male, 6−8 weeks of age) (Vital River Lab Animal Technology, Beijing, China) were maintained in the animal facility at the Institute of Materia Medica under specific pathogen-free (SPF) conditions. The sample size was predetermined empirically according to previous experience using the

same strains and treatments. For animal studies, mice were ear-marked before grouping and then were randomly distributed into groups by an independent researcher. The investigators were not blinded to mouse allocation during experiments and outcome assessment. All animal procedures were conducted in accordance with the guidelines of ARRIVE and approved by the Institutional Committee for the Ethics of Animal Care and Treatment in Biomedical Research of the Chinese Academy of Medical Sciences and Peking Union Medical College (Permit No. 002802).

The mouse model of irreversible PF was generated by repetitive intratracheal BLM injury as previously described with some modification[7,24]. Briefly, mice were anesthetized with 400 mg/kg avertin i.p. (Sigma−Aldrich). Bleomycin (BLM) (1 U/kg, Nippon Kayaku, Japan) in 50 μL of LPS-free PBS was instilled into the trachea 6 times, with 14 days between each challenge. Mice were sacrificed by excessive anesthesia on Day 40 after the last BLM challenge. The reversible PF model was generated by single intratracheal instillation of BLM (3 U/kg) in 50 μL of LPS-free PBS, and the mice were sacrificed by excessive anesthesia at the indicated time points after exposure. The mouse model of silicosis was generated by intratracheal single dose of 125 mg/kg silica particle suspension (Sigma−Aldrich) as described previously[25]. Mice were sacrificed by excessive anesthesia on Day 50 after the SiO_2 challenge. Mice in the sham groups were intratracheally administered an identical volume of PBS. For therapeutic experiments, mice were administered the indicated agents intravenously every 3 days from Day 10 after the last BLM injury or on Day 50 after SiO_2 challenge; the mice were sacrificed by excessive anesthesia on Day 40 after the last BLM injury or on Day 80 after the SiO_2 challenge. For inhibition of Mdm2 in mice, the mice were administered MX69 at dose of 100 mg/kg/day (i.p.) for a period of 3 days after every BLM challenge and 3 days before the mice were sacrificed. To overexpressing Mdm2 in lung tissue, the mice were intratracheal instilled of lentivirus overexpressing *Mdm2* (1×10^7 TU/mouse) 10 days after the last BLM challenge. For knockdown *Slc34a2* in lung, the mice were intratracheal instilled of *Slc34a2*-shRNA lentivirus (1×10^7 TU/mouse) 10 days after the first and the last BLM challenge. To overexpressing Slc34a2 in lung tissue, the mice were intratracheal instilled of *Slc34a2* adenovirus (5×10^8 pfu/mouse) 10 days after the last BLM challenge.

2.3. Lung function measurement

Mice were anesthetized with 400 mg/kg Avertin i.p. and placed on a flexivent system (Flexivent, SCIREQ Inc., Montreal, Canada). Mice were mechanically ventilated with a tidal volume of 10 mL/kg, a respiratory rate of 150 breaths/min and 3 cm H_2O positive end-expiratory pressure (PEEP) for evaluating lung function as described previously[26]. Dynamic pulmonary compliance was measured by Snapshot-150 perturbation.

2.4. Isolation of primary AEC2s

Primary mouse lung epithelial cells were isolated as described previously[27]. In brief, mice were sacrificed by excessive anesthesia and cleaned with 70% ethanol. The left and right ventricles were perfused with cold PBS until the lungs turned white. The lungs were lavaged with 1 mL of cold PBS 3 times and then perfused with 1 mL of dispase (1 mg/mL; Roche) and 0.5 mL of warm 1% low melt agarose (ThermoFisher). The lungs were removed, and each lobe was cut from the main stem bronchi. The lobes were digested in a 50-mL tube containing dispase (1 mg/mL) at room temperature for 45 min. The lobes were transferred into another 50-mL tube containing 10 mL of DMEM and 50 U/mL DNase (Sigma−Aldrich); then, the lung tissue was dissociated by pipetting up and down. The cells were filtered with 100-μm, 70-μm, 40-μm, and 20-μm cell strainers. The red blood cells were removed using ACK lysis buffer (ThermoFisher). The cells were harvested by centrifuging at $550 \times g$ for 5 min, and the lung cells were re-suspended in 500 μL of DMEM with 50 U/mL DNase. To remove the lineage cells, lung cells were incubated with biotinylated antibodies against CD45 (leukocytes, BioLegend 103104), CD16/32 (monocytes/macrophages, NK cells and neutrophils, BioLegend 101303), CD31 (endothelial cells, BioLegend 102504), Ter 119 (erythroid cells, BioLegend 116204), and integrin $\beta 4$ (club cells, distal lung progenitor cells and lineage-negative epithelial stem/progenitor cells, BioLegend 346-11A) for 60 min on ice. At the end of the incubation, the cells were washed with DMEM and re-suspended in 500 μL of DMEM with 50 U/mL DNase. The cells were then incubated with streptavidin-labeled magnetic beads (2.5 μL of SA MyOne T1 beads/1×10^6 cells) for 30 min on a rotator, and the lineage-positive cells were removed by a magnetic separator. The isolated cells were then cultured in a 10-cm dish for 45 min at 37 °C to make the fibroblast adherence, and the suspended AECs were collected by centrifuging at $550 \times g$ for 5 min. Newly isolated AECs were used for FACS sorting and Mdm2 activity detection. The AECs were labeled with anti-streptavidin-PE antibodies (BioLegend 405204) and anti-EpCAM-APC antibodies (BioLegend 118214), and the $DAPI^-$ live, Lin^-EpCAM^+ cells were sorted. Human $CD31^-CD45^-EpCAM^+HTII\text{-}280^+$AEC2s were isolated from single-cell suspensions of broncho alveolar lavage fluid (BALF) from patients with PF. For protein analysis, the sorted cells were lysed with radioimmunoprecipitation assay (RIPA) buffer. For other assays, the newly isolated AEC2s were cultured on fibronectin-coated dishes with DMEM containing 10% fetal bovine serum (FBS) supplemented with insulin/transferrin/selenium, non-essential amino acids, 0.25 μg/mL amphotericin B, 100 IU/mL penicillin, and 100 μg/mL streptomycin for 2 days.

2.5. Matrigel culture of AEC2s

5×10^3 flow-sorted mouse AEC2s were cultured in 100 μL of Matrigel/DMEM (1:1) mixture containing 2×10^5 MLg2908 cells. The Matrigel/DMEM mixture was plated into 0.4-μm Transwell chambers. A volume of 500 μL of culture medium was added to the lower chamber and was changed every day. The culture medium contained DMEM supplemented with insulin/transferrin/selenium, 10% FBS, 0.25 μg/mL amphotericin B, 100 IU/mL penicillin, and 100 μg/mL streptomycin. Colonies with a diameter of $\geq$50 μm were counted using a Zeiss Axiovert 40 inverted microscope, and the colony-forming efficiency (CFE) was determined by the ratio of the number of colonies to the number of input AEC2s on Day 14 after plating. For the phosphate feeding experiment, the Matrigel was mixed with phosphate-free DMEM (Gibco 11971025, 1:1), and phosphate-free DMEM culture medium was added to the lower chambers with different concentrations of phosphate buffer (mixture of Na_2HPO_4 and NaH_2PO_4, pH 7.4). For the detection of the level of *Aqp5* mRNA level, the Matrigel/DMEM chambers were infused with cell recovery solution (Corning), and the colonies were collected by centrifuging at $550 \times g$ for 5 min. Total RNA in the colonies was prepared using TRIzol reagent (Invitrogen).

2.6. Isolation of primary mouse lung fibroblasts

Primary mouse lung fibroblasts were isolated as described previously[28]. In brief, mice were sacrificed by excessive anesthesia and cleaned with 70% ethanol. The lung tissue was collected and washed with sterile PBS. Cut the tissue into ~1 mm pieces using scalpel and digested with Liberase Blendzyme 3 (Roche) at 37 °C for 60 min. After centrifuged at 550 × *g* for 5 min, the pellet was resuspended with DMEM/F12 media with 15% FBS, and cultured at 37 °C in a 10-cm dish. The dish was checked every day for fibroblasts growth, and the fibroblasts were harvested for passage or other assays after 7−14 days culture.

2.7. Phosphate concentration evaluation

Mice were sacrificed by injection with an overdose of Avertin and lavaged with 1 mL of sterilized saline through a 20-gauge angiocatheter inserted into the trachea. BALF from patients with PF or from patients without chronic inflammatory lung diseases were obtained from Beijing Friendship Hospital (Supporting Information Table S1). All the subjects gave appropriate informed consent to participate in this study. The study design was approved by the institutional ethical committee. Briefly, 50 mL of sterilized saline at body temperature was instilled through the bronchoscope. Mucus was removed from the fluid by filtration through two sheets of gauze. The BALF was centrifuged for 10 min at 400 × *g* at 4 °C. Phosphate concentration was measured with a Phosphate Colorimetric Assay Kit (BioVision) following the manufacturer's instructions. For intracellular phosphate determination, 1×10^6 AEC2s were washed with cold saline twice and suspended in 1 mL of double-distilled water. The suspension was sonicated for 30 s six times at 10 s intervals. The samples were centrifuged for 15 min at 4 °C at 12,000 × *g*, and intracellular phosphate in the supernatant was measured.

2.8. Assay of in vitro ubiquitination

Purified SLUG protein (200 ng, OriGene) was pre-incubated with MDM2 protein (200 ng, Millipore) on ice for 30 min. The SLUG/MDM2 complexes were incubated with a 20 μL reaction mixture containing some or all of the following components: E1 (200 ng, Boston Biochem, USA), UbcH5c (500 ng, OriGene), Ubiquitin (10 μg, Origene), 2 μL of a 10 × reaction buffer (Boston Biochem), and ATP (4 mmol/L, Boston Biochem). The reaction was carried out at 37 °C for 60 min with continuous agitation. Purified TRIB3-GST protein (300 ng, SinoBiological Inc.) was then added, followed by additional incubation (30 min). After the reaction was complete, the mixture was boiled in 5 × sample buffer, resolved by 10% SDS-PAGE and immunoblotted with an antibody against SLUG (CST 9585) or MDM2 (abcam ab16895).

2.9. Assays of E2-ubiquintin conjugate, MDM2 binding and discharge

Formation of E2-ubiquintin conjugate were performed as described previously[29]. Purified E2 (UbcH5c), E1, ubiquitin, and ATP were incubated at 37 °C for 6 h in reaction buffer (25 mmol/L Tris−HCL [pH 7.6] containing 5 mmol/L $MgCl_2$ and 100 mmol/L NaCl). For the *in vitro* binding assays, purified MDM2 and TRIB3 proteins were pre-incubated at 4 °C for 30 min. Then, the MDM2 protein and E2-Ub conjugate were mixed at 37 °C for 1 h in PBS buffer containing 0.2% Tween 20 and 2 mmol/L DTT. The reaction mixtures were precipitated with Protein A/G Plus-Agarose (Santa Cruz) and MDM2 antibody (abcam ab16895) at 4 °C overnight and then washed four times with PBS buffer. The bound proteins were eluted with 2 × SDS loading buffer and detected by immunoblot (IB). To analyze the discharge, E2-Ub conjugate and purified MDM2 were mixed. TRIB3 protein was then added and incubated with the mixture in 50 mmol/L MES (pH 6.5) at 37 °C for 6 h. The disappearance of the E2-Ub conjugate was analyzed by IB using an E2 antibody (abcam ab106315).

2.10. MDM2 binding protein identification

For protein identification *via* mass spectrometry, AEC2 from PBS- or BLM-treated mice were isolated, and the cell lysates were extracted and immunoprecipitated with anti-MDM2 antibody (abcam ab16895) using a Pierce Co-IP Kit (ThermoScientific 26149, USA). The eluents were separated on an SDS-PAGE gel followed by silver staining, and the bands were extracted from the gel and subjected to LC−MS/MS sequencing and data analysis by QLBio Biotechnology Co., Ltd. (Beijing, China). In brief, the proteins were digested in the gel and extracted. The digestion products were separated by a 120/60 min gradient elution at a flow rate of 0.600 L/min with the EASY-nLC 1000 system, which was directly interfaced with the Thermo Orbitrap Fusion mass spectrometer. The mass of the peptides was identified by an LC−MS/MS Q Exactive Hybrid Quadrupole-Orbitrap Mass Spectrometer (Thermo Scientific, USA). The MS/MS data were compared against a UniProt protein FASTA file using an in-house Proteome Discoverer (Version PD1.4, Thermo-Fisher Scientific, USA). Only peptides assigned to a given protein group were considered unique. The proteins that bound to Mdm2 in fibrotic AEC2s but not in healthy AEC2s are listed in Supporting Information Table S2.

2.11. RNA sequencing and analysis

Total RNA from AEC2s from mice was obtained, and the RNA quantity and quality were measured using a NanoDrop ND-1000. Libraries were constructed according to standard Illumina protocols. The quality of the RNA and complementary DNA was monitored using an Agilent Bioanalyzer 2100, and sequencing was performed on an Illumina HiSeq 4000 by KangChen Biotech Company (Shanghai). The series numbers are GSE110430 and GSE110479 in this study.

2.12. Analysis of surface plasmon resonance

Binding kinetics between TRIB3 and indicated peptides were measured by surface plasmon resonance using a BIAcore T200 instrument (GE Healthcare, Pittsburgh, USA) as described previously[23]. The dissociation constant (K_D) was calculated according to the BIA-evaluation software. Langmuir module was used to determine the K_D for all the peptides.

2.13. Circular dichroism analysis

Far-UV circular dichroism (300−190 nm) experiments were performed using a Jasco J-815 spectrometer equipped with a Jasco PTC-423S/15 temperature system consisting of a Peltier type constant-temperature cuvette holder and temperature controller (Jasco Corporation, Japan). Indicated peptides were dissolved in water for circular dichroism analysis. The conditions of measurement were as follows: 0.5 nm step resolution, 50 nm/min speed, 6 accumulations, 1 s response, 20 °C and 1 mm path length.

All spectra were the average of 6 accumulations after background subtraction and converted to a uniform scale of molar CD extinction coefficients. The contents of secondary structures were calculated using the built-in algorithms (Eq. (1)):

$$\text{mol. CD} = \frac{\text{CD (mdeg)}}{l \times c \times 32980} \quad (1)$$

2.14. Analysis of cellular uptake of peptides

Lung epithelial cells were treated with indicated concentrations of FAM-conjugated peptides for 24 h. The intracellular peptide was detected by flow cytometer (BD).

2.15. Statistics

Data are expressed as the mean ± standard error of the mean (S.E.M.). Comparisons between two groups were performed by unpaired two-tailed Student's *t*-test. One-way ANOVA with Bonferroni's multiple comparison test was used to analyze multiple groups with equal variances, and Kruskal−Wallis one-way ANOVA was used to analyze multiple groups with unequal variances. The correlations among groups were determined by Pearson's correlation test. Generally, all assays were carried out with $n \geq 3$ biological replicates. $P < 0.05$ was considered statistically significant.

2.16. Data availability

The datasets generated during and/or analyses during the current study are available from the corresponding author on reasonable request.

3. Results

3.1. Repetitive lung injury elevates slug expression causing LAR failure

To determine the role of LAR in PF development, we generated 2 mouse models of lung injury with fibrosis change by either single or multiple intratracheal instillation of bleomycin[7] (sBLM or mBLM). sBLM mice developed acute lung injury and PF on Day 21, but the lesion regressed spontaneously on Day 45 after BLM challenge, with a steady restoration of lung function; however, mBLM mice showed progressive lung injury with fibrosis change indicated by septal thickening, loss of alveolarization and a progressive decline in lung function (Supporting Information Fig. S1A and S1B). The AEC2 to AEC1 transition is a crucial process in LAR[10,13,14]. Thus, we examined the expression of NKX2.1 and Hopx in fibrotic lung tissue, both of which are expressed in intermediate cells during trans-differentiation from AEC2 to AEC1[30]. The $NKX2.1^{+}HOPX^{+}$ AEC2s were increased on Day 45 after sBLM challenge; however, this realveolarization did not occur after mBLM challenge (Fig. S1C). The proliferation of AEC2s in sBLM or mBLM mice was either increased or decreased on Day 45 after BLM challenge (Fig. S1D). To determine AEC2 differentiation, the mBLM PF model was generated in *Sftpc-Cre:ROSA-EYFP* mice. The doxycycline treatment led to lineage labeling of approximately 77%−86% pro-SPC positive cells (Supporting Information Fig. S2A). The number of elongated $EYFP^{+}$ AEC1s differentiated from AEC2s in mBLM mice was comparable with that in control mice after tracing for 3 months (Fig. 1A). Because AEC2s can show the stemness *in vitro*, we isolated primary AEC2s from mouse lung tissue, and these high purity AEC2s contained few P63- or KRT5-positive basal cells or lineage-negative epithelial stem/progenitor cells (Fig. S2B and S2C). AEC2 colonies were observed after 12 days (Fig. 1B) and further differentiated into AEC1s (Fig. 1C) in a 3D culture system, indicating the LAR ability. AEC2s from mBLM mice (mBLM AEC2s) displayed markedly lower colony-forming efficiency (CFE) and a smaller colony size than AEC2s from sham mice (sham AEC2s) (Fig. 1D−F). The proliferation and differentiation of AEC2s were enhanced after the first bleomycin exposure, but this enhancement receded after the fourth bleomycin exposure, as indicated by a decrease in Ki67 and NKX2.1/HOPX staining (Supporting Information Fig. S3A and S3B). Indeed, the expression of AEC2-related genes was suppressed, while that of AEC1-related genes was disordered in mBLM AEC2s (Fig. 1G). These data suggest that repetitive lung injury causes LAR failure and progressive PF.

The morphology of mBLM AEC2s was changed from squamous to spindle-shaped after adherent culture in fibronectin-coated culture dishes (Fig. 2A). These AEC2s expressed lower E-cadherin levels compared with sham AEC2s (Fig. 2B). Consistently, the expressions of Snail and Slug but not those of TWIST and ZEB1, which are all E-cadherin repressors[31], were increased in mBLM AEC2s (Fig. 2C). We thus examined whether SNAIL or SLUG contributed to the dysfunction of AEC2s in PF. The CFE of AEC2s was reduced with *Slug* overexpression but not with *Snail*, *Twist* or *Zeb 1* overexpression (Fig. 2D). Additionally, the colonies formed by mBLM AEC2s exhibited higher Slug and lower PDPN expression levels compared with those from control mice (Fig. 2E). Slug-overexpressing AEC2s showed reduced expression of development- and differentiation-related genes but enhanced expression of inflammation- and injury repair-related genes (Fig. 2F). Furthermore, the expression of SLUG in AEC2s returned to a normal level after a transient increase in sBLM mice, but a progressive elevation of SLUG expression was found in mBLM AEC2s (Fig. 2G, Supporting Information Fig. S3C). Consistent with this finding, $Slug^{-/-}$ mice showed fewer fibrotic changes (Fig. 2H and I) and better lung function (Fig. 2J) in response to mBLM challenge than wild type (WT) mice. The number of $NKX2.1^{+}HOPX^{+}$ cells and the CFE of AEC2s from $Slug^{-/-}$ mBLM mice were higher than those in cells from WT mBLM mice (Fig. 2K and L). To evaluate the contribution of Slug in AEC2s on fibroblast activation, we examined secretion phenotype of AEC2s isolated from mBLM mice. The concentrations of IL-23, IL-25, IL-33, TNF-α, IL-1β, and TGF-β were higher in the culture supernatant of mBLM AEC2s than that of control mice (Supporting Information Fig. S4A). While, the levels of IL-25, IL-33, IL-1β, and TGF-β were significantly lower in $Slug^{-/-}$ AEC2s compared with that in WT AEC2s after mBLM exposure (Supporting Information Fig. S4A). The supernatant from mBLM AEC2s not only stimulated migration (Fig. S4B) and proliferation (Fig. S4C) of lung fibroblasts, but also enhanced the secretion of collagen Iα1 (Fig. S4D). Indeed, the AEC2s isolated from $Slug^{-/-}$ mBLM mice lost the pro-fibrotic features (Fig. S4B−S4D). These *in vivo* and *in vitro* data not only indicate that SLUG in AEC2s is crucial for PF development but also show that elevated SLUG expression in AEC2s causes LAR failure during chronic lung injury.

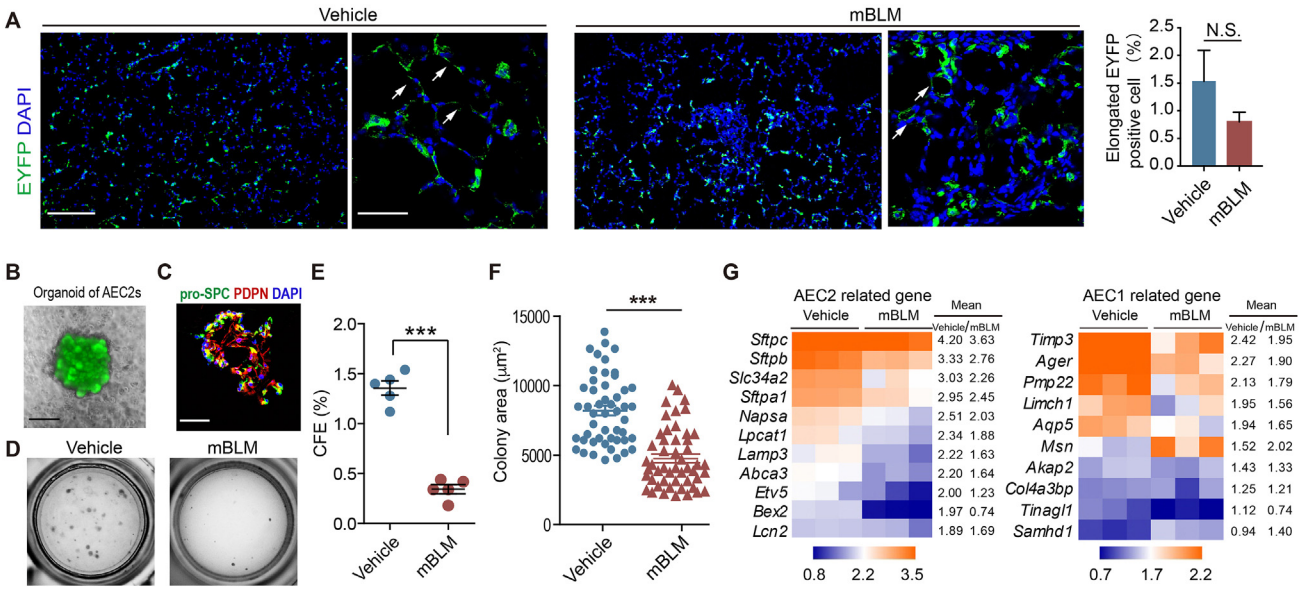

Figure 1 Chronic lung injury causes LAR failure. (A) Confocal images showing the lineage-traced AEC2s in lung tissues from Sftpc-Cre; ROSA-EYFP mice 10 days after multiple vehicle or BLM exposure ($n = 3$). Scale bars, 200 μm (left) and 50 μm (right). N.S.: not significant. (B) Representative colony formation by AEC2s from Sftpc-Cre; ROSA-EYFP mice in a 3D co-culture system on Day 14. Scale bars, 50 μm. (C) Confocal images showing the pro-SPC and PDPN expression in AEC2 colonies ($n = 4$). Scale bars, 50 μm. (D) Images of the indicated AEC2 colonies growing in a 3D co-culture system ($n = 3$). (E) Colony-forming efficiency of AEC2s sorted from vehicle- or mBLM-challenged mice ($n = 5$). (F) Colony sizes of AEC2s from vehicle- or mBLM-challenged mice ($n = 50$). (G) Heatmap showing the expression of AEC2- or AEC1-related genes in AEC2s sorted from vehicle- or mBLM-challenged mice ($n = 3$). The color scale indicates a lg ratio of the normalized RNA-seq value intensities. Statistical significance between the two groups was determined by unpaired two-tailed Student's *t*-test. ***$P < 0.001$.

3.2. *SLUG inhibits LAR by repressing SLC34A2 mediated phosphate homeostasis*

Given that chronic lung injury reduces the expression profile of the development- and differentiation-related genes in AEC2s, we suspected that elevated SLUG expression might repress the expression of these genes. We found that the mRNA expression of *Slc34a2* but not *Etv5*, *Bex2*, *Sftpa1*, *Sftpb*, *Sftpc*, *ABCA3*, *LAMP3*, *Napsa*, and *Lpcat1* which are down-regulated in fibrotic AEC2s (Fig. 1G), was repressed in *Slug*-overexpressed AEC2s (Fig. 3A). Additionally, the protein expression of Slc34a2 was reduced in mBLM AEC2s (Fig. 3B), and which was negatively correlated with that of SLUG (Fig. 3C and D). SLC34A2 is a sodium-dependent phosphate transporter. Reduced SLC34A2 expression has been observed in AEC2s from IPF patients[12], and a loss-of-function mutation in *SLC34A2* causes pulmonary alveolar microlithiasis[32]. We reasoned that SLUG might suppress AEC2 self-renewal and differentiation by repressing SLC34A2 expression. We found that overexpression of SLUG reduced the promoter luciferase activity of *SLC34A2* (Fig. 3E). Additionally, SLUG repressed the expression of *SLC34A2* by binding to the M2 region in the promoter of *SLC34A2,* which contains two putative SLUG binding sites (Fig. 3F and G). Indeed, chromatin immunoprecipitation (ChIP) of SLUG-Myc was enriched for one conserved promoter region of *SLC34A2* (−297 to −178), and the putative SLUG DNA binding motif in this region was well conserved across species (Fig. 3H and I). In addition, the phosphate level was significantly higher in BALF from patients with PF than in that from patients without chronic lung disease (Fig. 3J and Table S1) and from mBLM mice (Fig. 3K). In contrast, the intracellular phosphate level was decreased in mBLM AEC2s (Fig. 3L).

Notably, the CFE was reduced in *Slc34a2*-knockdown AEC2s (Fig. 4A) but was increased with elevated extracellular phosphate concentrations in a phosphate-free culture medium (Fig. 4B). Phosphorus is a critical element for biological function, especially for intracellular signal transduction and energy production[33]. We found that phosphorylation of ERK1/2, P38 and JNK was increased in AEC2s isolated from sBLM-exposed mice but not in mBLM AEC2s (Fig. 4C). The p38 inhibitor SB203580 and the JNK inhibitor SP600125, but not the MEK1/2 inhibitor PD0325901, decreased the CFE of AEC2s (Fig. 4D), suggesting that activation of these two kinases is crucial for LAR. The levels of phosphorylated p38 and JNK were increased on Day 7 after sBLM exposure, and this elevation persisted for 3 weeks. Similar to sBLM injury, the enhanced phosphorylation of P38 and JNK could be found at the 10th day after the 3rd bleomycin exposure but decreased from the 10th day after the 4th bleomycin exposure in the mBLM model (Fig. 4E). To verify the role of SLC34A2 in LAR, we instilled *Slc34a2* adenovirus into lung tissue 10 days after mBLM challenge. We found that overexpression of Slc34a2 in lung tissue not only reduced collagen deposition and the hydroxyproline content in lung tissue (Fig. 4F–H) but also enhanced the CFE of mBLM AEC2s (Fig. 4I). Moreover, silencing *Slc34a2* expression interfered with the resolution of PF (Fig. 4J–L), disrupted phosphate homeostasis (Fig. 4M and N), reduced the levels of p-P38 and p-JNK (Fig. 4O), and suppressed AEC2 self-renewal in mBLM-exposed $Slug^{-/-}$ mice (Fig. 4P). These data indicate that reduced SLC34A2 expression decreases the intracellular phosphate concentration, which hinders the phosphorylation of JNK and P38 MAPK in AEC2s and mediates SLUG-suppressed LAR in PF.

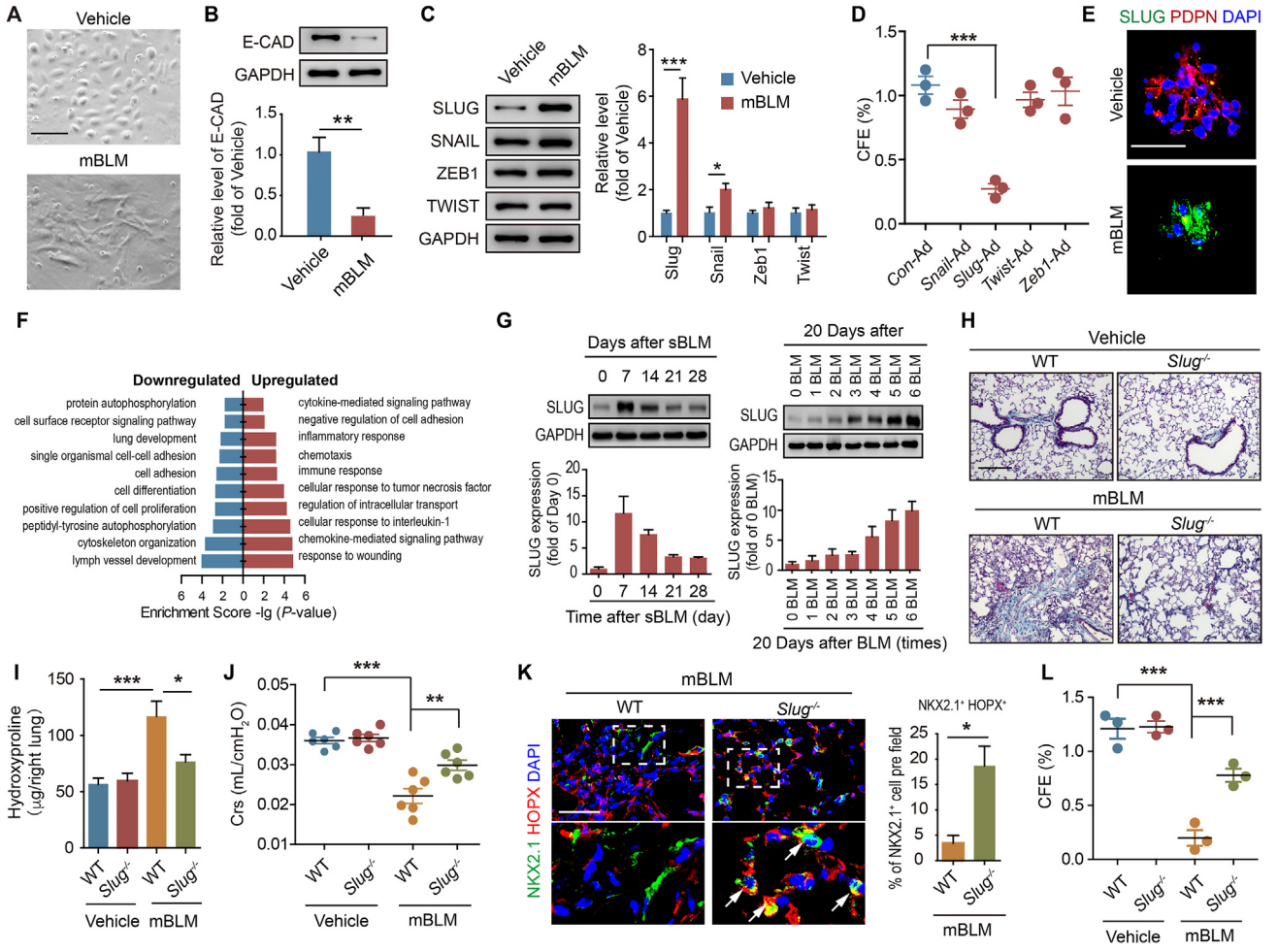

Figure 2 SLUG suppresses differentiation of AEC2s into AEC1s in PF. (A) Sample phase contrast micrographs showing the morphology of AEC2s sorted from vehicle- or mBLM-challenged mice ($n = 3$). Scale bars, 100 μm. (B) Semi-quantification analysis showing E-cadherin (E-cad) expression in AEC2s sorted from the indicated mice ($n = 3$). GAPDH was used as the loading control. (C) Sample immunoblots and semi-quantitative analyses of the expression of E-cadherin repressors in AEC2s sorted from the indicated mice ($n = 3$). GAPDH was used as the loading control. (D) The CFE of AEC2s infected with the indicated adenovirus ($n = 3$). (E) Confocal images showing Slug and PDPN expression in colonies formed by AEC2s sorted from vehicle- or mBLM-challenged mice ($n = 3$). Scale bars, 50 μm. (F) Gene ontology analyses of *Slug*-adenovirus-infected AEC2s versus *Con*-adenovirus-infected AEC2s. The top 10 significant upregulated and downregulated GO terms and their enrichment scores are displayed. (G) Immunoblotting of Slug in AEC2s from mice at the indicated days post BLM challenges ($n = 3$). GAPDH was used as the loading control. (H–J) Masson staining (H), hydroxyproline content in the right lung (I), and Crs (J) were assessed to evaluate the fibrotic changes and lung function in lungs from WT and $Slug^{-/-}$ mice after mBLM exposure ($n = 6$). Scale bars, 200 μm. (K) Co-localization of the AEC2 marker NKX2.1 and AEC1 marker Hopx in lung tissues from WT or $Slug^{-/-}$ mice after mBLM challenge ($n = 3$). Scale bars, 50 μm. (L) The colony-forming efficiency of AEC2s sorted from WT or $Slug^{-/-}$ mice after mBLM challenge ($n = 3$). Statistical significance between the two groups was determined by unpaired two-tailed Student's *t*-test; Statistical significance among groups was determined by one-way ANOVA. $^{*}P < 0.05$, $^{**}P < 0.01$, $^{***}P < 0.001$.

3.3. *Loss of MDM2 function impedes SLUG degradation*

Because chronic lung injury did not enhance the mRNA expression of *Slug* in mBLM AEC2s (Fig. 5A), we assumed that the elevated Slug expression might be due to its abnormal degradation. SLUG degradation was suppressed by the ubiquitin–proteasome system (UPS) inhibitor MG132 but not by the autophagy inhibitor 3 MA (Fig. 5B). Indeed, ubiquitinated Slug was reduced in AEC2s from mBLM-challenged mice and from SiO_2- exposed mice, another reliable PF mouse model (Fig. 5C and D). Among the four E3 ubiquitin ligases that catalyze SLUG ubiquitylation, MDM2, FBXW8, FBXL14, and β-TRCP[34–37], only MDM2 was elevated in mBLM AEC2s (Fig. 5E). MDM2 elevation was detected in AEC2s from PF patients and from mBLM and SiO_2 PF mice (Fig. 5F–H). Knockdown of *Mdm2* further decreased the mRNA level of E-cadherin in mBLM AEC2s (Fig. 5I). To determine whether the increased MDM2 in AEC2s is functional, we examined the catalytic activity of MDM2 using *in vitro* ubiquitination assay. The activity of MDM2 in fibrotic lung tissue was reduced, as indicated by the *in vitro* ubiquitinated Slug level (Fig. 5J). These data indicate that dysfunction of the E3 ligase MDM2 suppresses SLUG ubiquitination and degradation in PF.

To further detect the role of MDM2 in the development of PF, we treated the mice with MX69 which promoting MDM2 self-

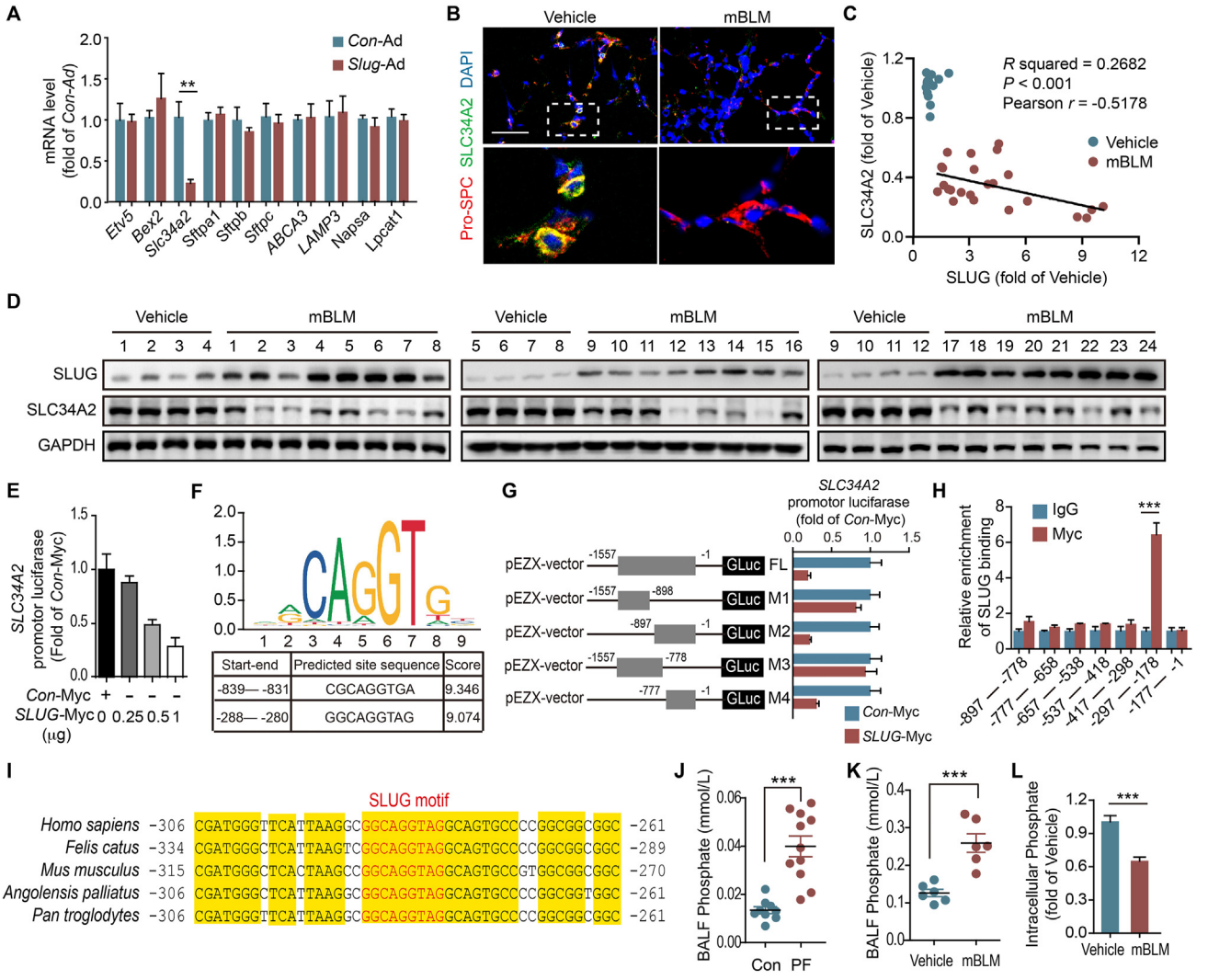

Figure 3 SLUG represses SLC34A2 expression by binding to the *Slc34a2* promoter. (A) Quantitative analyses of mRNA expression of the AEC2 maturation-related genes in Slug-overexpressing AEC2s ($n = 3$). (B) Confocal images showing the pro-SPC and SLC34A2 expression in lung tissues from mBLM challenged mice ($n = 5$). Scale bars, 50 μm. (C, D) Correlation between Slug expression and Slc34a2 expression in lungs after mBLM challenge. The *Y*-axis denotes the relative Slc34a2 expression, and the *X*-axis denotes the relative Slug expression. Each point represents the value from one mouse. The *P* value was calculated with Spearman's rank correlation test in the mBLM group (C, vehicle, $n = 12$; mBLM, $n = 24$). Sample immunoblots of the expression of SLUG and SLC34A2 in lungs from vehicle- or mBLM-exposed mice (D). (E) Relative expression of *SLC34A2* promoter-driven luciferase reporters in *SLUG*-overexpressing primary human alveolar epithelial cells (PHAECs) ($n = 3$). (F) Canonical SLUG binding motif in the promoter of *SLC34A2* gene obtained by JASPAR. (G) The relative expression of the truncated *SLC34A2* promoter-driven luciferase reporters in *SLUG*-overexpressing PHAECs ($n = 3$). (H) ChIP analysis of Slug binding to the *SLC34A2* promoter in PHAECs ($n = 3$). (I) Schematic depiction of the *SLC34A2* promoter with putative Slug binding sites. (J, K) The phosphate concentration in BALF from patients with PF (J, Con $n = 9$; PF, $n = 11$) and from mBLM-exposed mice (K, $n = 6$). (L) The phosphate concentration in AEC2s isolated from the indicated mice ($n = 6$). Statistical significance between the two groups was determined by unpaired two-tailed Student's *t*-test. $^{**}P < 0.01$, $^{***}P < 0.001$.

ubiquitination and protein degradation[38]. Significant fibrotic change in lung tissue was found in the mice treated with MX69 after mBLM challenging (Supporting Information Fig. S5A). However, inhibition of MDM2 did not induce PF without BLM injury (Fig. S5A). Inhibition of MDM2 after lung injury significantly increased the hydroxyproline content in the lungs and decreased the lung function of fibrotic mice (Fig. S5B and S5C). MX69 treatment decreased the protein level of MDM2, and increased the level of Slug in AEC2s isolated from fibrotic mice but not control mice (Fig. S5D), further suggesting that MDM2 promotes Slug degradation during the development of PF. Meanwhile, the capacity of AEC2s mediated LAR was further declined in MX69 treated group (Fig. S5E). In addition, we enhanced the Mdm2 function following mBLM exposure through intratracheal instillation of lentivirus overexpressing *Mdm2*. Overexpressing MDM2 in lung attenuated PF (Fig. S5F and S5G), and improved lung function of the fibrotic mice (Fig. S5H). Furthermore, we found that the Slug level was decreased (Fig. S5I), and the self-renewal capacity of mBLM AEC2s was restored in *Mdm2* overexpressed mBLM AEC2s (Fig. S5J).

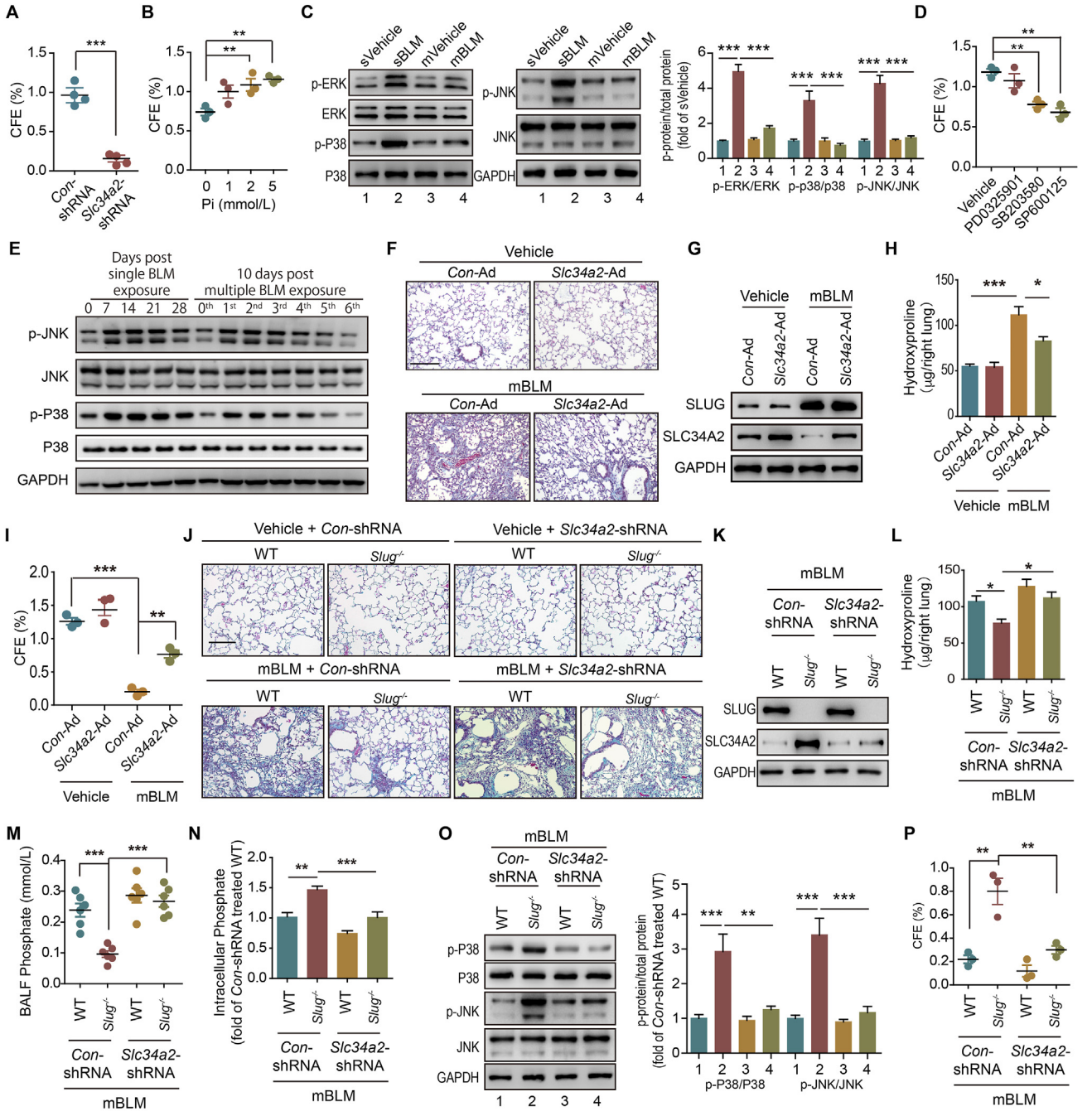

Figure 4 Reduced SLC34A2 mediates SLUG-induced LAR failure and PF. (A) The CFE of AEC2s infected with lentiviral particles containing *Con*-shRNA or *Slc34a2*-shRNA ($n = 4$). (B) The CFE of AEC2s cultured with the indicated concentrations of phosphate ($n = 3$). (C) Sample immunoblots showing the expression of the indicated proteins in AEC2s from the mice after sBLM exposure for 40 days or from the mice after mBLM exposure for 40 days ($n = 5$). (D) The CFE of AEC2s in the presence of MEK1/2 (PD0325901), P38 (SB203580) or JNK (SP600125) inhibitor ($n = 3$). (E) Sample immunoblots showing the expression of the indicated proteins in AEC2s from the mice at different timepoints post sBLM or mBLM exposure ($n = 3$). (F) Masson staining was performed to evaluate fibrotic changes in lungs from mBLM-exposed mice after intratracheal instillation of *Slc34a2* adenovirus ($n = 6$). Scale bars, 200 μm. (G) Sample immunoblots of the expression of SLUG and SLC34A2 in AEC2s sorted from the indicated mice ($n = 3$). GAPDH was used as the loading control. (H) Hydroxyproline content in the right lung of the indicated mice ($n = 6$). (I) The colony-forming efficiency of AEC2s sorted form the indicated mice ($n = 3$). (J) Masson staining was performed to evaluate PF after intratracheal instillation of *Slc34a2*-shRNA lentivirus in mBLM-exposed WT mice or Slug$^{-/-}$ mice ($n = 5$). Scale bars, 200 μm. (K) Sample immunoblots of the expression of SLUG and SLC34A2 in AEC2s sorted from the indicated mice ($n = 3$). GAPDH was used as the loading control. (L) Hydroxyproline content in the right lung of the indicated mice ($n = 5$). (M) The phosphate concentration in BALF from the indicated mice ($n = 6$). (N) The phosphate concentration in AEC2s isolated from the indicated mice ($n = 6$). (O) Sample immunoblots of the expression of the indicated proteins in AEC2s ($n = 5$). (P) The CFE of AEC2s from the indicated mice ($n = 3$). Statistical significance between the two groups was determined by unpaired two-tailed Student's *t*-test; Statistical significance among groups was determined by one-way ANOVA. $^*P < 0.05$, $^{**}P < 0.01$, $^{***}P < 0.001$.

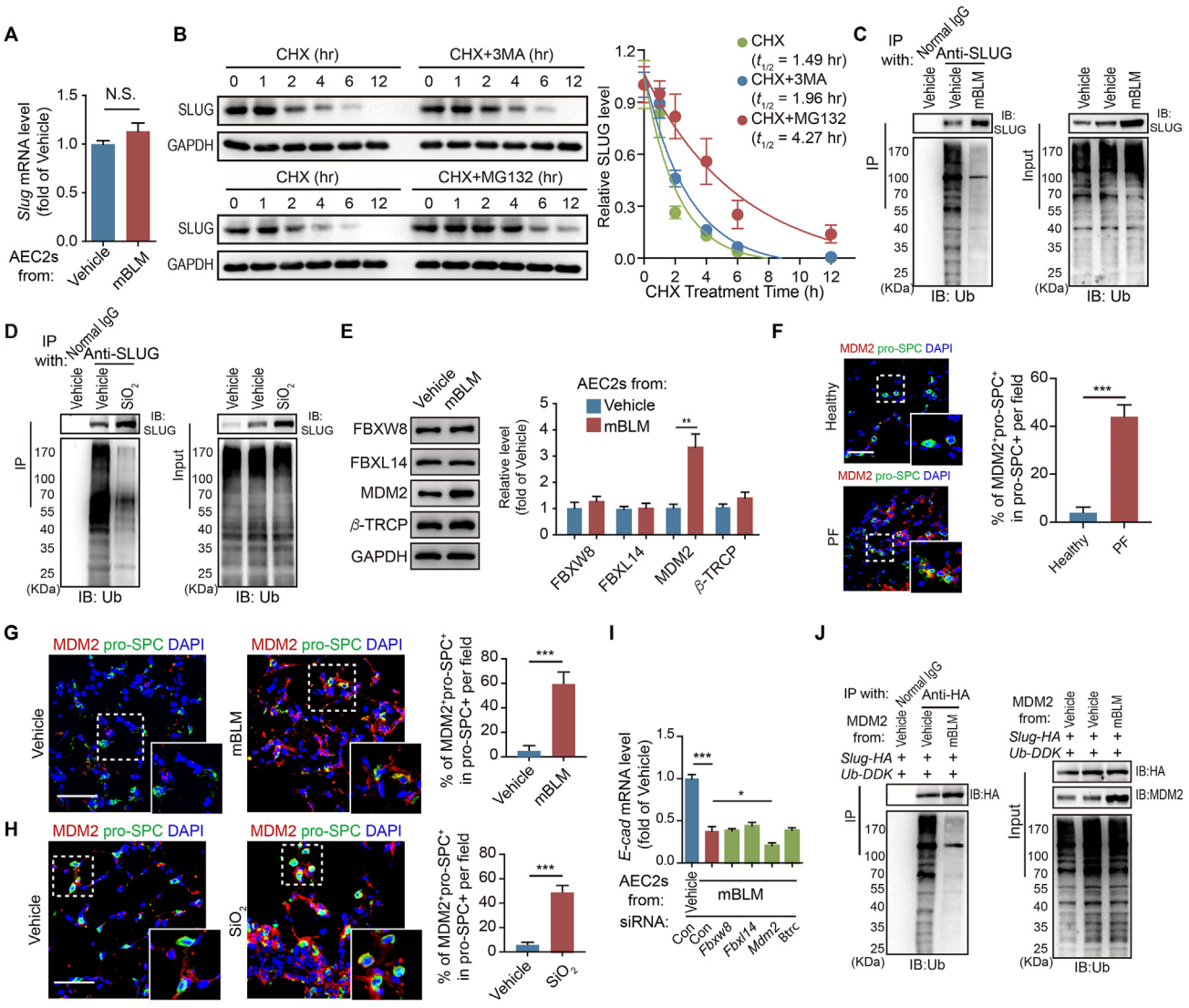

Figure 5 Dysfunction of MDM2 suppresses SLUG degradation. (A) Quantitative analyses of *Slug* mRNA content in AEC2s from the indicated mice. N.S.: not significant. (B) Quantitative analyses of SLUG degradation in AEC2s in the presence of protein synthesis inhibitor cycloheximide (CHX) (10 μg/mL) and 3 MA (5 mmol/L) or MG132 (10 μmol/L). The half-lives ($t_{1/2}$) of Slug degradation were calculated by one phase decay analysis ($n = 3$). GAPDH was used as the loading control for IB. (C, D) IP assay analyses of ubiquitinated Slug in lung tissues from mBLM mice (C) and SiO_2-challenged mice (D) ($n = 5$). (E) Protein levels of Slug-related E3 ligases in AEC2s sorted from the indicated mice ($n = 3$). GAPDH was used as the loading control for IB. (F−H) Confocal images showing the co-localization of MDM2 and pro-SPC in lung tissues from PF patients (F) and from mice after mBLM (G) or SiO_2 (H) exposure ($n = 3$). Scale bars, 50 μm. (I) *E-cad* mRNA levels in sorted AEC2s after transfection with the indicated siRNA ($n = 3$). (J) Sample immunoblots showing the E3 activity of MDM2 in AECs from mBLM mice in the presence of E1, E2 (UbcH5c), Ub, ATP, and subtract (SLUG) ($n = 3$). Statistical significance between the two groups was determined by unpaired two-tailed Student's *t*-test; Statistical significance among groups was determined by one-way ANOVA $^*P < 0.05$ $^{**}P < 0.01$, $^{***}P < 0.001$.

3.4. *TRIB3 disturbs MDM2-mediated SLUG degradation*

Using mass spectrum analysis, 24 proteins were identified as binding with Mdm2 in fibrotic AEC2s but not in normal AEC2s (Fig. 6A and Supporting Information Table S2). Among these Mdm2-binding proteins, Trib3 is a stress sensor involved in inflammatory diseases, including tissue fibrosis, by interacting with cellular signaling and functional proteins[39−41], and its expression was increased in the lungs of PF patients (Fig. 6B and C) and in mBLM AEC2s (Fig. 6D). Endogenous TRIB3 interacted with MDM2 in lung epithelial cells (Fig. 6E), and this was confirmed by GST pull-down assays (Fig. 6F) and by colocalization of MDM2 with TRIB3 in fibrotic lung tissues from PF patients (Fig. 6G) and from mBLM or SiO_2 PF mice (Fig. 6H and I). Because SLUG interacted with MDM2 at residues 211−300[36], we constructed a series of MDM2 deletion mutants to examine whether TRIB3 binds MDM2 in the same region (Supporting Information Fig. S6A). TRIB3 interacted with the zinc- and RING-finger domains of MDM2, suggesting that TRIB3 binds with MDM2 next to the SLUG binding region, and the inhibitory effect of TRIB3 on the SLUG/MDM2 interaction might be due to steric hindrance between these two proteins (Fig. S6A). The MDM2-binding region of TRIB3 was located at the C-terminal region within the KD domain (Fig. S6B). Additionally, TRIB3 impeded the SLUG/MDM2 interaction in a concentration-dependent manner (Fig. 6J).

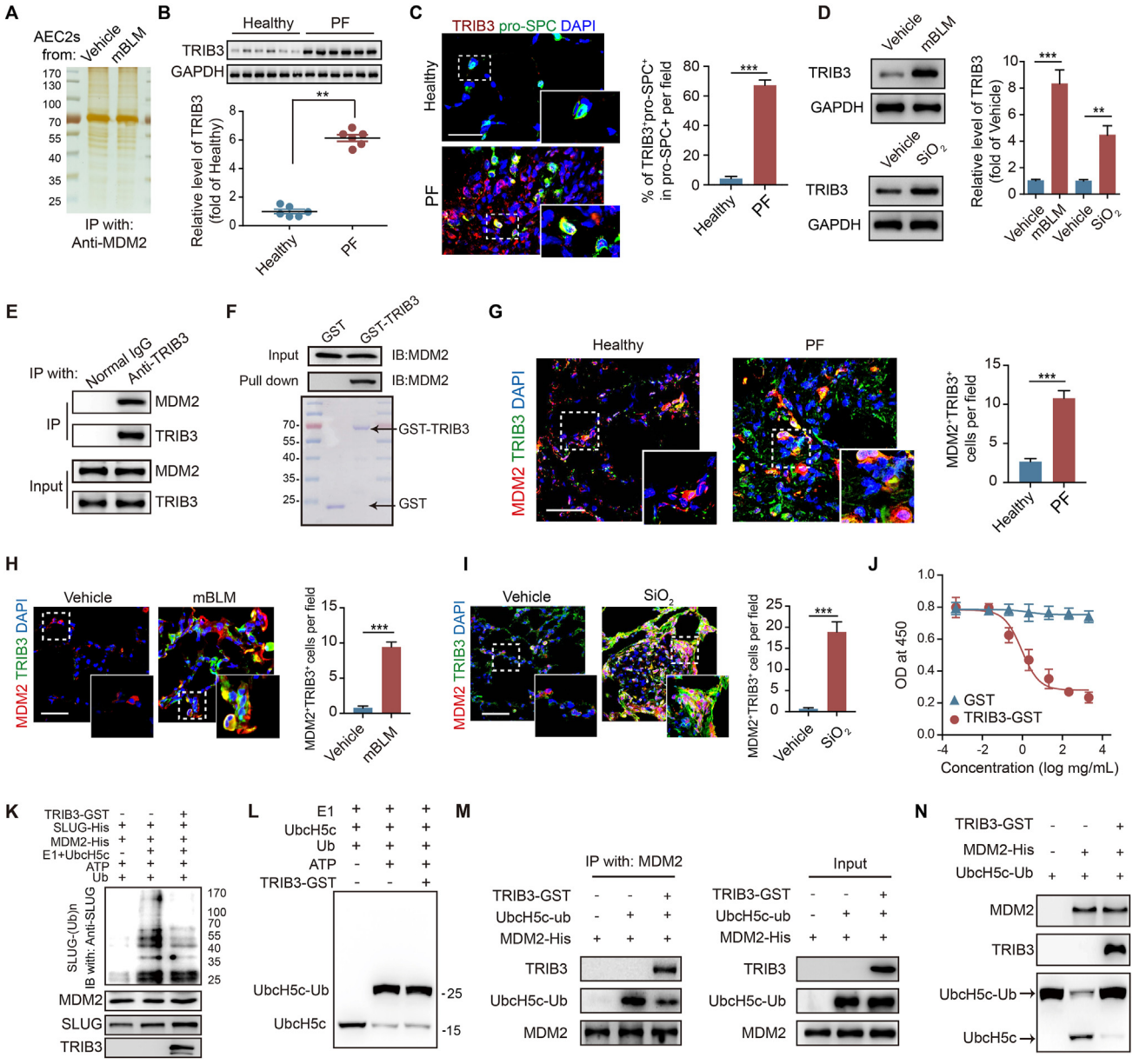

Figure 6 MDM2 inhibits SLUG degradation by physically interacting with TRIB3. (A) AEC2s were sorted form lung tissues of the vehicle- or mBLM-exposed mice. AEC2s lysate was IP with anti-Mdm2 antibody, and silver-staining shows the MDM2 binding proteins in AEC2s. (B) Quantitation of TRIB3 expression in lung samples from healthy controls or patients with pulmonary fibrosis (PF) ($n = 6$). GAPDH was used as the loading control for immunoblotting. (C) Sample confocal images showing co-localization of TRIB3 and pro-SPC in lung tissues from PF patients ($n = 3$). Scale bars, 50 μm. (D) The protein level of TRIB3 in AEC2s was detected with IB ($n = 3$). GAPDH was used as the loading control for IB. (E) IP assay analyses of the TRIB3/MDM2 interaction in lung epithelial cells. Cells extracts were IP with normal IgG or anti-TRIB3 antibody (Ab) and blotted with anti-MDM2 Ab ($n = 3$). (F) GST pull-down assay showing *in vitro* interaction of TRIB3/MDM2 ($n = 3$). GST-only protein was used as the negative control. GST fusion proteins were stained with Coomassie Blue. (G–I) Confocal images showing the co-localization of MDM2 and TRIB3 in lung tissues from PF patients (G) and in lung tissues from the mice after mBLM (H) or SiO_2 injury (I) ($n = 3$). Scale bars, 50 μm. (J) Competitive ELISA analyses of binding of SLUG to MDM2 in the presence of TRIB3-GST or GST-tagged protein ($n = 3$). (K) Sample immunoblots showing the E3 activity of MDM2 in the presence of E1, E2 (UbcH5c), Ub, ATP, and subtract (SLUG), plus or minus TRIB3, *in vitro* ($n = 3$). (L) Sample immunoblots showing UbcH5c−Ub conjugation in the presence of E1, Ub, and ATP plus or minus TRIB3 *in vitro* ($n = 3$). (M) Sample immunoblots showing the binding ability of MDM2 to UbcH5c−Ub ($n = 3$). (N) Sample immunoblots showing UbcH5c−Ub conjugation in the presence of TRIB3 ($n = 3$). Statistical significance between the two groups was determined by unpaired two-tailed Student's *t*-test. $^{**}P < 0.01$, $^{***}P < 0.001$.

We verified whether the TRIB3 interaction with the RING domain of MDM2 reduced the E3 ubiquitin ligase activity of MDM2 using an *in vitro* ubiquitination assay. Recombinant MDM2 readily produced ubiquitinated SLUG in the presence of E1, ATP, UbcH5c, and ubiquitin. When recombinant TRIB3 was added to the reaction system, the ubiquitination of SLUG was

suppressed (Fig. 6K), suggesting that TRIB3 interacts with MDM2 and interferes with MDM2-catalyzed ubiquitination. The UPS degradation process requires the consecutive action of E1, E2 and E3 ubiquitin enzymes[42]. In the presence of TRIB3, E1 enzymes activated ubiquitin and conjugated it to E2 enzymes (Fig. 6L). However, TRIB3 reduced the association of ubiquitin-conjugated E2 enzymes with MDM2 (Fig. 6M) and prevented MDM2-induced liberation of ubiquitin from the E2−ub complexes (Fig. 6N). Indeed, neither overexpressing nor silencing *Trib3* affected *Slug* transcription in AEC2s (Supporting Information Fig. S7A). Instead, *Trib3* overexpression prolonged the half-life of SLUG degradation (Fig. S7B). Moreover, colocalization of SLUG and TRIB3 was found in fibrotic lungs (Fig. S7C).

3.5. *Knockout of TRIB3 in AEC2s prevents PF development*

To verify the critical role of TRIB3 in PF pathogenesis *via* MDM2-mediated SLUG degradation in AEC2s and SLUG-mediated LAR failure in PF, we generated AEC2-specific *Trib3*-deficient mice by crossing mice containing a floxed *Trib3* exon 3 with mice expressing Cre-recombinase under control of the *Sftpc* promoter (referred to as *Sftpc-Cre; Trib3*$^{flox/flox}$). These mice were viable and fertile and were born at the expected Mendelian ratio without apparent abnormalities in adult mice. Knockout of *Trib3* in AEC2s reduced Slug expression, prevented PF development and restored the self-renewal capacity of mBLM AEC2s (Supporting Information Fig. S8A−S8D). Moreover, the concentration of phosphate in BALF was lower and the intro-AEC2s phosphate level was higher in *Sftpc-Cre*; *Trib3*$^{flox/flox}$ mice in comparison with WT mice (Fig. S8E and S8F). Knockout *Trib3* in AEC2s also increased the phosphorylation of P38 and JNK post mBLM injury (Fig. S8G). More importantly, *Sftpc-Cre;Trib3*$^{flox/flox}$ mice showed significant protection following challenge with intratracheal instillation of SiO_2 indicated by the reductions in SLUG expression in AEC2s (Fig. S8H) and fibrotic changes in lung tissues (Fig. S8I and S8J); enhances in CFE of AEC2s (Fig. S8K), phosphate homeostasis (Fig. S8L and S8M) and the phosphorylation of p-P38 and p-JNK (Fig. S8N).

3.6. *Disturbing the TRIB3/MDM2 interaction restores LAR and reduces PF*

Given that the TRIB3/MDM2 interaction stabilizes SLUG to suppress LAR in PF, disturbing this interaction might be a promising therapeutic strategy for PF. We screened the zinc-finger and RING-finger domains of MDM2 with the I-TASSER server to predict the MDM2 secondary structure. In total, four α-helix structures were found in the TRIB3-binding domain, but only MR2 (seq. 460−470) and MR3 (seq. 409−417) were at least 9 amino acids (AA) in length (Fig. 7A). MR2 and MR3 were synthesized with N-terminal and C-terminal protective AA (Fig. 7A), and their binding ability with TRIB3 was measured. MR2 displayed a high affinity for TRIB3 (K_D = 46.0 ± 2.1 nmol/L), whereas there was no interaction between MR3 and TRIB3 (Fig. 7B). To determine whether MR2 disturbed the TRIB3/MDM2 interaction to accelerate SLUG degradation, a fusion peptide, PMR2, was designed by linking the cell-penetrating peptide Pep 2 to MR2[43]. Similarly, PMR3 was generated as a control peptide by connecting Pep2 to MR3. Both PMR2 and PMR3 could penetrate lung epithelial cells (Fig. 7C and D), but only PMR2 disturbed the TRIB3/MDM2 interaction (Fig. 7E) and enhanced the association of SLUG with MDM2 (Fig. 7F). Additionally, PMR2 increased the SLUG ubiquitination (Fig. 7G) and caused SLUG degradation in an UPS-dependent manner (Fig. 7H). Furthermore, we observed whether PMR2 can break the known protein−protein interactions mediated by TRIB3 or MDM2. We found that PMR2 only interrupted the MDM2/MDMX[44] interaction but not the interactions of MDM2/p53[45], MDM2/PML[23], TRIB3/AKT[46], TRIB3/p62[40], and TRIB3/SMAD3[47] (Supporting Information Fig. S9A−S9F).

To overcome the shortcomings of a natural α-helix peptide for potential therapy against PF[48], three all-hydrocarbon staple MR2 peptides were designed to reinforce the α-helical structure and enhance cell penetration. The i+4 stapled analogs of MR2 sequences (named SMR1/2/3) were synthesized (Fig. 8A), and these stapled peptides showed higher affinity for MDM2 in comparison with PMR2 (Fig. 8B). The highest helix-ratio peptide SMR3 not only showed a better druggability than PMR2 (Fig. 8C, Supporting Information Fig. S10A and S10B) but also restored TRIB3- suppressed AEC2 self-renewal and differentiation (Fig. S10C and S10D).

SMR3 readily penetrated AEC2s (Fig. S10E) and exhibited a good safety profile (Fig. S10F−S10H). It reduced collagen deposition, inflammation (Fig. 8D, Supporting Information Fig. S11A) and hydroxyproline levels (Fig. 8E, Fig. S11B) and improved lung function (Fig. 8F, Fig. S11C) in mBLM mice and SiO_2 mice. SMR3 reduced Slug expression but enhanced Slc34a2 expression in AEC2s (Fig. 8G, Fig. S11D). Additionally, SMR3 increased AEC2 proliferation and promoted the AEC2/AEC1 transition in lung tissue from mBLM mice (Fig. 8H and I, Fig. S11E and S11F). Moreover, SMR3 improved the self-renewal and differentiation capacities of AEC2s from fibrotic mice or PF patients in comparison with those from control mice or patients (Fig. 8J−L, Fig. S11G−S11I). Importantly, SMR3 restored phosphate homeostasis (Fig. S11J−S11M) and phosphorylated capacity of P38 and JNK in AEC2s from both mBLM- and SiO_2-induced PF mice (Fig. S11N and S11O). In sum, the stapled peptide SMR3 is a highly selective, stable and cell-penetrable leading compound with a potent therapeutic efficacy and thus could be further developed for therapy directed at LAR against PF (Fig. 8M).

4. Discussion

Recent studies indicate that acute lung injury caused acute PF is reversible after the removal of inciting damage, such as virus infection or a single intratracheal BLM administration[5,6,13]. However, repetitive lung epithelium injury is commonly considered an initiating factor in irreversible PF[49]. LAR failure not only leads to progressive PF[13] but is also a critical reason for the limited efficacy of disease-modifying therapy in IPF and across progressive lung alveolar diseases[50]. In this study, we found that the acute PF in a sBLM mouse model is the self-recovery process because of the restored regenerative capacity of AEC2s[13]. In contrast, this recoverable LAR is not observed both in an irreversible PF model and in IPF patients. The repeated alveolar damage is one of the important prerequisites for the occurrence of fibrotic diseases in lung, so the mBLM model is more in line with the mechanism of clinical pulmonary fibrosis[7]. At the same time, the pathological changes of the mBLM model were closer to those of clinical patients with PF. Importantly, we showed that repetitive lung injury causes progressive augmentation of Slug protein in AEC2s, which represses AEC2s from transition into AEC1s and interferes with PF resolution. Moreover, the Slug high expressed AEC2s may serve as driving force to trigger the fibroblast activation. Genetic inhibition

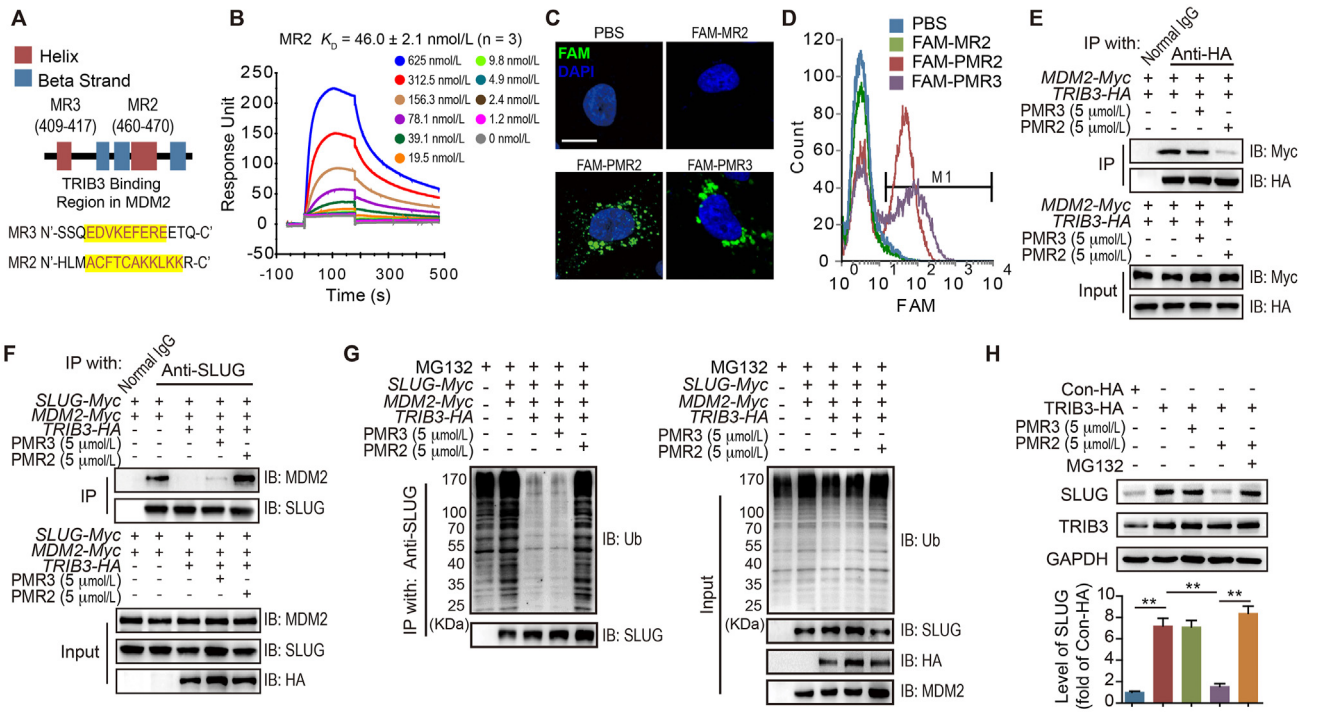

Figure 7 Disturbing the TRIB3/MDM2 interaction promotes SLUG degradation. (A) I-TASSER server analyses of the secondary structure of the TRIB3 binding region in MDM2 and the peptide sequences containing the indicated α-helical sequence and protective AA. Highlighted sequence is the α -helix structure in the peptides. (B) Surface plasmon resonance (SPR) analyses of the kinetic interaction between MR2 and TRIB3 ($n = 3$). (C, D) Sample immunofluorescence image (C) and flow cytometry plot (D) showing the cellular penetration of MR2, PMR2 and PMR3 conjugated with FAM ($n = 3$). Scale bars, 20 μm. (E) Sample immunoblot shows PMR2 but not PMR3 disturbing the interaction of TRIB3/MDM2 in primary human alveolar epithelial cells (PHAECs) ($n = 3$). (F) Sample immunoblot showing PMR2 restoring the interaction of MDM2/SLUG in PHAECs ($n = 3$). (G) Sample immunoblots showing PMR2 but not PMR3 restoring the TRIB3-suppressed ubiquitination of SLUG in cells ($n = 3$). (H) Quantitative analyses of SLUG and MDM2 expression in TRIB3-overexpressing PHAECs treated with 5 μmol/L PMR3 or PMR2 or 10 μmol/L MG132 ($n = 3$). GAPDH was used as the loading control for IB. Statistical significance among groups was determined by one-way ANOVA. $^{**}P < 0.01$.

of Slug expression and accelerated Slug degradation partially restored LAR capacity and reduced PF. In addition, the microenvironment of lung alveolar niche induced by chronic lung injury prohibits epithelial repair also[7]. Thus, the abnormal function of AEC2 cells and the dysregulated alveolar microenvironment together inhibits the process of LAR. The repeated alveolar epithelial injury leads to persistent chronic inflammation, and the molecular mechanism of this inflammation is very different from that caused by acute lung injury. The immune microenvironment after acute lung injury can lead to rapid self-renewal and differentiation of AEC2 cells. However, our study shows that AEC2 cells in chronic PF have reduced stemness and themselves become a source of inflammation that promotes fibrosis progression. The AEC2 cells dysfunction may be the result of repeated injury of lung alveoli, and may also be the consequence of changes in the immune microenvironment. This change includes the interaction between different types of cells in alveoli such as inflammatory cells, fibroblasts, and vascular endothelial cells, and includes the regulation of the systemic inflammation on the local injury lung tissue.

SLUG, a member of the SNAIL family of transcriptional repressors, plays an important role in embryonic development by regulating stem cell function[20,51]. However, Slug overexpression has been reported to lead to cancer stem cell traits in several cancer types, including breast, ovarian, and intestinal cancer, by repressing E-cadherin expression and activating epithelial−mesenchymal transition (EMT)[52,53]. Nevertheless, it has been illustrated that SLUG decreases the self-renewal of hematopoietic stem cells[54]. In this study, we found that Slug inhibits the AEC2/AEC1 transition and self-renewal of AEC2s from mice with irreversible PF. We observed that enhanced Slug stability suppresses the LAR capacity of AEC2s by repressing the expression of Slc34a2, a sodium-dependent phosphate transporter. Slc34a2 gene mutation or loss of function can disrupt phosphate homeostasis and directly induce pulmonary alveolar microlithiasis in which calcium phosphate crystal formation in the alveolar space results in progressive PF and respiratory failure[32], and reduced expression of this type IIb sodium-phosphate transporter has been found in AEC2s from patients with PF[12]. Notably, we found that reduced SLC34A2 expression inhibits phosphate influx in AEC2s, which impedes the phosphorylation of JNK and P38 MAPK, two crucial kinases for supporting LAR[55]. Our work thus identifies the SLUG−SLC34A2 axis serving as a link between the chronic injury of AEC2s and LAR failure in PF. It is well known that SLUG plays an important role in cancer by promoting EMT. We found that SLUG induces mesenchymal-like transition in AEC2 cells. The function of AEC2 cells undergoing EMT in the pathogenesis of PF are currently unclear, since AEC2 cells undergoing EMT are not an important source of myofibroblasts in PF[56]. Our results found that the mesenchymal-like changed AEC2 cells are important source of inflammation, which triggers fibroblast activation by releasing profibrotic factors. Therefore, AEC2 cells

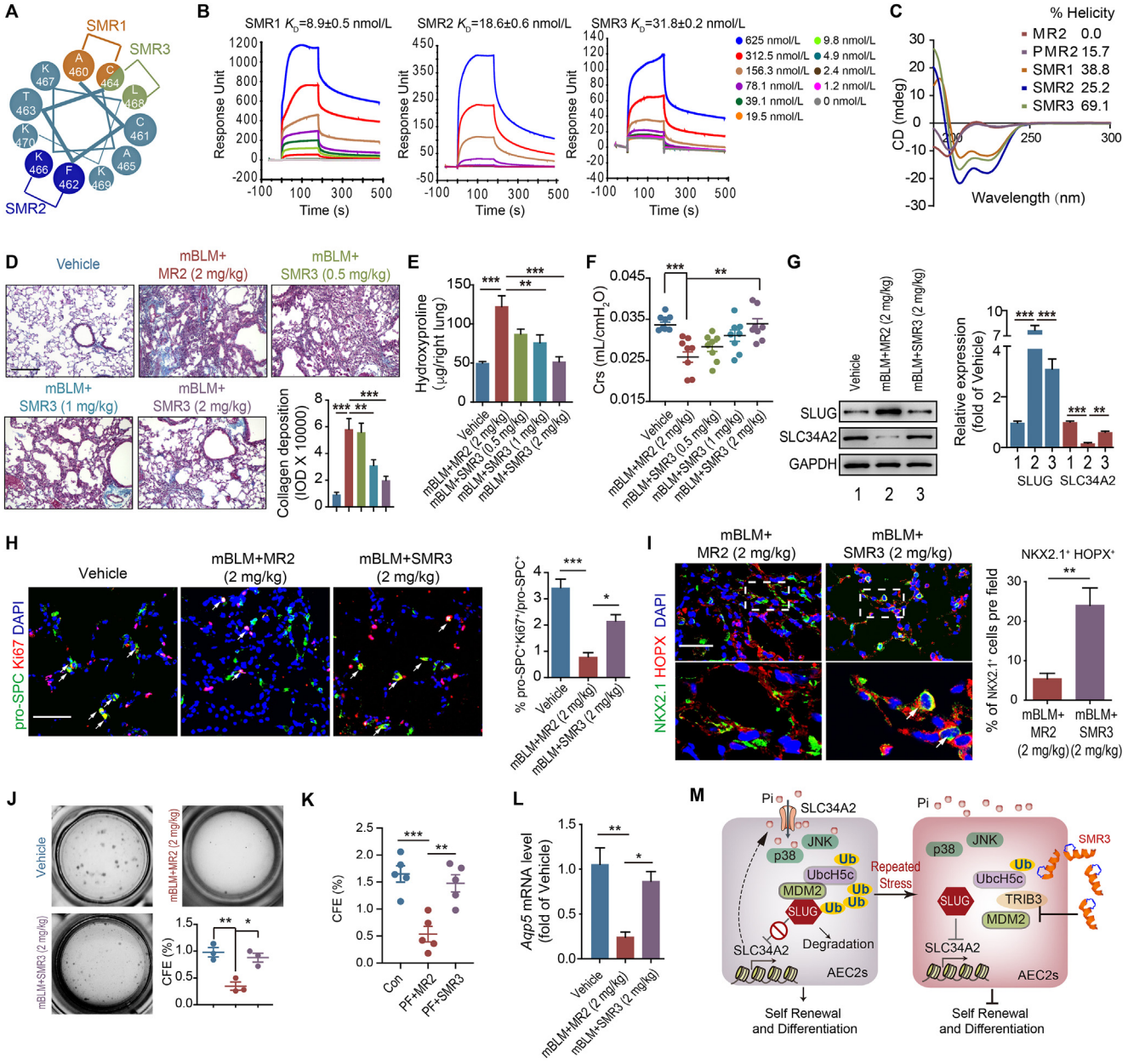

Figure 8 Targeting SLUG degradation restores LAR and reduces PF. (A) Structural analysis of the stapled MR2 peptide helices. (B) The indicated concentration of stapled MR2 peptides was passed over immobilized TRIB3 on CM5 sensor chips, and the kinetic interaction of the peptides with TRIB3 was determined by SPR analysis ($n = 3$). (C) The helicity of the peptides was detected *via* circular dichroism analysis. (D–F) Masson staining (D), hydroxyproline content in the right lung (E), and Crs (F) were assessed to evaluate PF and lung function ($n = 8$). Scale bars, 200 μm. (G) Sample blots show the expression of Slug and Slc34a2 in AEC2s from the indicated mice ($n = 5$). (H) Co-staining and quantification of pro-SPC and Ki67 in lung tissues from fibrotic mice ($n = 3$). Scale bars, 50 μm. (I) Co-localization of the AEC2 marker NKX2.1 and AEC1 marker HOPX in lung tissues from mBLM-challenged mice ($n = 3$). Scale bars, 50 μm. (J) Images of the indicated AEC2 colonies growing in a 3D co-culture system and the colony-forming efficiency of AEC2s from vehicle or mBLM-challenged mice ($n = 3$). (K) The colony-forming efficiency of AEC2s from patients with or without PF treated with SMR3 (5 mmol/L) ($n = 5$). (L) The *Aqp5* mRNA level in colonies formed by AEC2s from the indicated mice ($n = 3$). (M) Schematic diagram illustrating that MDM2 dysfunction-induced Slug accumulation promotes PF development by inhibiting LAR and that the anti-fibrotic role of SMR3 results from disturbance of the TRIB3/MDM2 interaction. Statistical significance between the two groups was determined by unpaired two-tailed Student's *t*-test; Statistical significance among groups was determined by one-way ANOVA. $^*P < 0.05$, $^{**}P < 0.01$, $^{***}P < 0.001$.

that develop EMT are likely to promote PF disease progression with a profibrotic phenotype.

The bleomycin model of PF is partly driven by enhanced TGF-β signaling, and the cooperation with TGF-β-activated SMAD3 determines SLUG transcription and activity[19]. In addition to this classical signaling pathway, few studies have investigated the post-transcriptional modification of SLUG in PF. This study is mainly focus on the protein stability and the biological function of

SLUG. As a transcriptional factor, SLUG is an extremely labile protein, and its protein level in cells is tightly controlled by posttranslational modification, particularly *via* the UPS[57,58]. Indeed, the low level of SLUG in healthy tissue is due to its fast degradation; once SLUG degradation is impeded, its transcriptional regulatory effects are amplified and sustained[36]. In this study, we found that the stress sensor TRIB3 interacts with MDM2, a RING-finger-dependent E3 ubiquitin ligase, to reduce SLUG degradation and impede AEC2 stemness, which the importance of MDM2 in SLUG stabilization. A previous study indicated that MDM2 is required for SLUG degradation in cancer cells[36]. However, there are other E3 ligases, including FBXW8, FBXL14, and β-TRCP, that belong to the F-box protein family and can mediate SLUG degradation[34,35,37]. Unlike RING-finger-dependent E3 ligases, F-box protein family E3 ligases need to form a Skp, Cullin, and F-box-containing complex (SCF complex) to ubiquitinate their substrates[59]. We did not find these F-box proteins to be involved in SLUG accumulation in AEC2s from fibrotic lung tissue. TRIB3 interacts with the RING-finger domain of MDM2 to inhibit the E3 ubiquitin ligase activity of MDM2. Additionally, TRIB3 interacts with the zinc-finger domain of MDM2, which causes the disassociation of SLUG from MDM2. Thus, the TRIB3/MDM2 interaction induces a double inhibition of MDM2-mediated SLUG degradation. Therefore, our current work provides novel insights into the role of UPS in the regulation of LAR and PF development. Besides ubiquitination, the protein stability and activity of SLUG are also determined by other post-transcriptional modification such as phosphorylation and SUMOylation[60,61]. Thus, further studies are needed to evaluate the relationship of these modifications of SLUG and LAR.

Although TRIB3 does not have the ability to phosphorylate other proteins, it acts as an accomplice *via* interaction with intracellular signaling or functional proteins to control fundamental processes extending from mitosis and cell activation to apoptosis and the modulation of gene expression[39,62,63]. We recently reported that TRIB3 promotes invasion and migration across human cancer cells by interacting with SMAD3 to promote TGF-β1-induced EMT[47]. Interestingly, Tomcik et al.[41] recently explored the profibrotic role of TRIB3 in renal tissue and systemic sclerosis through the activation of TGF-β1 signaling. In addition, we have found that TRIB3 promotes liver fibrosis by inhibiting autophagy in hepatic stellate cells[64]. These observations support our finding that TRIB3 plays a critical role in PF pathogenesis. In this study, we found that TRIB3 promotes PF by interacting with MDM2 and interfering with its E3 ubiquitin ligase function. This action prolongs SLUG degradation, leading to LAR failure. Therefore, we believe that TRIB3 in fibroblasts promotes pulmonary fibrosis progression by inducing fibroblast activation, while TRIB3 in alveolar epithelial cells impedes pulmonary fibrosis recovery by inhibiting lung regeneration. Our previous work indicated that TRIB3 interacts with P62, a selective autophagic receptor, to suppress the degradation of several cancer-promoting factors[40], and TRIB3 interacts with PML-RARα, thus promoting acute promyelocytic leukemia progression *via* inhibition of PML-RARα degradation[23]. Also, we found that the interaction of TRIB3/GSK3β maintains the pro-fibrotic phenotype of macrophage[65]. These studies suggest that TRIB3 is a critical modulator of intracellular protein quality control systems.

Substantial progress has been made in the treatment of PF using disease-modifying therapies instead of anti-inflammatory agents. A number of compounds targeting extracellular matrix deposition, tyrosine kinases, and the immune system have undergone clinical trials, raising hopes for new clinical therapies for IPF[66]. Although epithelial or stem cell transplantation shows some definite benefits for IPF patients[15,16], there is no reliable drug targeting LAR. This may be due to the fact that the molecular mechanism of LAR failure is still unclear, especially in response to chronic inflammation. Also, the effect of these anti-fibrotic medicines on LAR is totally unknown. Besides promoting LAR, the inhibition of EMT, epithelial cells apoptosis, epithelial cells senescence, or pro-fibrotic factors releasing from AEC2s may contribute to the change of PF also. Thus, targeting the dysfunctional or injured AEC2s in fibrotic lung tissue should be a defensible strategy to treating PF. Our study indicates that accelerating SLUG degradation in AEC2s is a promising therapy for PF by promoting AEC2/AEC1 transition. With this hypothesis, we translated the finding that interrupting the TRIB3/MDM2 interaction accelerates the clearance of SLUG and promotes LAR into an anti-fibrosis therapeutic strategy. We modified the α-helical peptide MR2 using a hydrocarbon stapling technique, which stabilized its α-helical structure and enhanced the cell penetrance ability, suggesting that this all-hydrocarbon stapling technique improved the pharmaceutical properties of this peptide by enhancing its K_D and stability. Indeed, disturbing the TRIB3/MDM2 interaction using this stapled peptide promoted AEC2 differentiation by accelerating Slug degradation and restoring Slc34a2 expression. Critically, this peptide exhibited a potent *in vivo* therapeutic efficacy in different self-recovery-limited PF models. Our work coincides with the observation that targeting protein−protein interactions is emerging as a therapeutic strategy for chronic diseases[67]. Considering that SLUG plays critical roles in the pathogenesis of PF and that Slug cannot feasibly be accessed by therapeutics such as antibodies or small molecular compounds, targeting of Slug degradation, as presented in the current study, may represent a significant therapeutic advance in the treatment of PF and other lung alveolar diseases. However, elucidation of the precise mechanism by which this peptide binds to the TRIB3/MDM2 complex requires further study. Additionally, whether the protective effects of this peptide are related to a more general effect of regulating the abundance of MDM2 substrates other than SLUG should be further studied.

5. Conclusions

In this study, we found that LAR failure is a consequence of post-transcriptional-regulated SLUG expression. Critically, the elevated expressions of SLUG in IPF alveolar epithelial cells suggest that the accumulation of SLUG is responsible for the dysfunction of AEC2s[12,18]. Although the roles of the Slug-supported epithelial−mesenchymal transition in PF are subject to debate, these cells can release large quantities of fibrogenic and inflammatory factors to activate resident fibroblasts to become myofibroblasts in pulmonary and renal fibrosis[68,69]. Indeed, we found that the proliferation and differentiation abilities of AEC2s are repressed and that the expression of Slc34a2 is reduced in Slug-positive AEC2s. In addition, Slug-positive AEC2s cannot further differentiate into AEC1s and lose self-renewal capacity. Thus, our work provides a potential mechanism to explain the phenotype of mesenchymal changed AEC2s in PF.

Acknowledgments

This work was supported by grants from National Key R&D Program of China (2017YFA0205400), National Natural Science

Foundation of China (82173875 to Xiaoxi Lv; 81973344 and 81673474 to Fang Hua), and from CAMS Innovation Found for Medical Sciences (2021-I2M-1−026 to Xiaoxi Lv), Non-profit Central Research Institute Fund of Chinese Academy of Medical Sciences (2022-JKCS-05 to Xiaoxi Lv), Fundamental Research Funds for the Central Universities (3332019150 to Tingting Zhang). This paper is dedicated to the memory of Prof. Zhuowei Hu (1955−2021, Institute of Materia Medica, Chinese Academy of Medical Sciences & Peking Union Medical College, Beijing, China), an outstanding pharmacologist and a respected teacher for our scientific career. We appreciate the invaluable suggestions and support from Prof. Zhuowei Hu.

Author contributions

Xiaoxi Lv raised conceptions and participated in the overall design, supervision and coordination of the study. Xiaoxi Lv and Shanshan Liu designed and performed most of experiments. Chang Liu, Tingting Zhang, Ke Li, Fang Hua, Jiaojiao Yu, Yuxin Liu, Xia Li, Li Li, and Bo Huang participated in molecular and cellular biological experiments. Bing Cui, Jie Qi, Jinmei Yu, and Xiaowei Zhang performed animal studies. Zhigang Yao collected clinical information and materials. Xiaoxi Lv, Shanshan Liu wrote the manuscript. All authors read and approved the manuscript.

Conflicts of interest

The authors declare no conflicts of interest.

Appendix A. Supporting information

Supporting data to this article can be found online at https://doi.org/10.1016/j.apsb.2023.01.008.

References

1. Putman RK, Hatabu H, Araki T, Gudmundsson G, Gao W, Nishino M, et al. Association between interstitial lung abnormalities and all-cause mortality. *JAMA* 2016;**315**:672−81.
2. Richeldi L, Collard HR, Jones MG. Idiopathic pulmonary fibrosis. *Lancet* 2017;**389**:1941−52.
3. King Jr TE, Bradford WZ, Castro-Bernardini S, Fagan EA, Glaspole I, Glassberg MK, et al. A phase 3 trial of pirfenidone in patients with idiopathic pulmonary fibrosis. *N Engl J Med* 2014;**370**:2083−92.
4. Richeldi L, du Bois RM, Raghu G, Azuma A, Brown KK, Costabel U, et al. Efficacy and safety of nintedanib in idiopathic pulmonary fibrosis. *N Engl J Med* 2014;**370**:2071−82.
5. Yao X, Luo T, Shi Y, He Z, Tang R, Zhang P, et al. A cohort autopsy study defines COVID-19 systemic pathogenesis. *Cell Res* 2021;**31**:836−46.
6. Mineo G, Ciccarese F, Modolon C, Landini MP, Valentino M, Zompatori M. Post-ARDS pulmonary fibrosis in patients with H1N1 pneumonia: role of follow-up CT. *Radiol Med* 2012;**117**:185−200.
7. Cao Z, Lis R, Ginsberg M, Chavez D, Shido K, Rabbany SY, et al. Targeting of the pulmonary capillary vascular niche promotes lung alveolar repair and ameliorates fibrosis. *Nat Med* 2016;**22**:154−62.
8. Degryse AL, Lawson WE. Progress toward improving animal models for idiopathic pulmonary fibrosis. *Am J Med Sci* 2011;**341**:444−9.
9. Basil MC, Katzen J, Engler AE, Guo M, Herriges MJ, Kathiriya JJ, et al. The cellular and physiological basis for lung repair and regeneration: past, present, and future. *Cell Stem Cell* 2020;**26**:482−502.
10. Barkauskas CE, Cronce MJ, Rackley CR, Bowie EJ, Keene DR, Stripp BR, et al. Type 2 alveolar cells are stem cells in adult lung. *J Clin Invest* 2013;**123**:3025−36.
11. Beers MF, Moodley Y. When is an alveolar type 2 cell an alveolar type 2 cell? A conundrum for lung stem cell biology and regenerative medicine. *Am J Respir Cell Mol Biol* 2017;**57**:18−27.
12. Xu Y, Mizuno T, Sridharan A, Du Y, Guo M, Tang J, et al. Single-cell RNA sequencing identifies diverse roles of epithelial cells in idiopathic pulmonary fibrosis. *JCI Insight* 2016;**1**:e90558.
13. Liang J, Zhang Y, Xie T, Liu N, Chen H, Geng Y, et al. Hyaluronan and TLR4 promote surfactant-protein-C-positive alveolar progenitor cell renewal and prevent severe pulmonary fibrosis in mice. *Nat Med* 2016;**22**:1285−93.
14. Jiang P, Gil de Rubio R, Hrycaj SM, Gurczynski SJ, Riemondy KA, Moore BB, et al. Ineffectual AEC2-to-AEC1 differentiation in IPF: persistence of KRT8(hi) transitional state. *Am J Respir Crit Care Med* 2020;**201**:1443−7.
15. Jacob A, Morley M, Hawkins F, McCauley KB, Jean JC, Heins H, et al. Differentiation of human pluripotent stem cells into functional lung alveolar epithelial cells. *Cell Stem Cell* 2017;**21**:472−88. e10.
16. Nadkarni RR, Abed S, Draper JS. Stem cells in pulmonary disease and regeneration. *Chest* 2018;**153**:994−1003.
17. Hill C, Jones MG, Davies DE, Wang Y. Epithelial−mesenchymal transition contributes to pulmonary fibrosis *via* aberrant epithelial/fibroblastic cross-talk. *J Lung Health Dis* 2019;**3**:31−5.
18. Jayachandran A, Konigshoff M, Yu H, Rupniewska E, Hecker M, Klepetko W, et al. SNAI transcription factors mediate epithelial−mesenchymal transition in lung fibrosis. *Thorax* 2009;**64**:1053−61.
19. Nieto MA. The snail superfamily of zinc-finger transcription factors. *Nat Rev Mol Cell Biol* 2002;**3**:155−66.
20. Guo W, Keckesova Z, Donaher JL, Shibue T, Tischler V, Reinhardt F, et al. Slug and Sox9 cooperatively determine the mammary stem cell state. *Cell* 2012;**148**:1015−28.
21. Phillips S, Kuperwasser C. SLUG: critical regulator of epithelial cell identity in breast development and cancer. *Cell Adhes Migrat* 2014;**8**:578−87.
22. Ruffenach G, Umar S, Vaillancourt M, Hong J, Cao N, Sarji S, et al. Histological hallmarks and role of Slug/PIP axis in pulmonary hypertension secondary to pulmonary fibrosis. *EMBO Mol Med* 2019;**11**:e10061.
23. Li K, Wang F, Cao WB, Lv XX, Hua F, Cui B, et al. TRIB3 promotes APL progression through stabilization of the oncoprotein PML-RARalpha and inhibition of p53-mediated senescence. *Cancer Cell* 2017;**31**:697−710. e7.
24. Lee SH, Lee EJ, Lee SY, Kim JH, Shim JJ, Shin C, et al. The effect of adipose stem cell therapy on pulmonary fibrosis induced by repetitive intratracheal bleomycin in mice. *Exp Lung Res* 2014;**40**:117−25.
25. Shimbori C, Shiota N, Okunishi H. Involvement of leukotrienes in the pathogenesis of silica-induced pulmonary fibrosis in mice. *Exp Lung Res* 2010;**36**:292−301.
26. Lv XX, Liu C, Liu SS, Li YX, Wang WY, Li K, et al. The cell cycle inhibitor P21 promotes the development of pulmonary fibrosis by suppressing lung alveolar regeneration. *Acta Pharm Sin B* 2022;**12**:735−46.
27. Sinha M, Lowell CA. Immune defense protein expression in highly purified mouse lung epithelial cells. *Am J Respir Cell Mol Biol* 2016;**54**:802−13.
28. Seluanov A, Vaidya A, Gorbunova V. Establishing primary adult fibroblast cultures from rodents. *JoVE* 2010;**44**:2033.
29. Choi JS, Park BC, Chi SW, Bae KH, Kim S, Cho S, et al. HAX1 regulates E3 ubiquitin ligase activity of cIAPs by promoting their dimerization. *Oncotarget* 2014;**5**:10084−99.
30. Liebler JM, Marconett CN, Juul N, Wang H, Liu Y, Flodby P, et al. Combinations of differentiation markers distinguish subpopulations of alveolar epithelial cells in adult lung. *Am J Physiol Lung Cell Mol Physiol* 2016;**310**:L114−20.
31. Lamouille S, Xu J, Derynck R. Molecular mechanisms of epithelial−mesenchymal transition. *Nat Rev Mol Cell Biol* 2014;**15**:178−96.
32. Saito A, Nikolaidis NM, Amlal H, Uehara Y, Gardner JC, LaSance K, et al. Modeling pulmonary alveolar microlithiasis by epithelial deletion of the Npt2b sodium phosphate cotransporter reveals putative

biomarkers and strategies for treatment. *Sci Transl Med* 2015;**7**:313ra181.
33. Chande S, Bergwitz C. Role of phosphate sensing in bone and mineral metabolism. *Nat Rev Endocrinol* 2018;**14**:637−55.
34. Fu J, Lv X, Lin H, Wu L, Wang R, Zhou Z, et al. Ubiquitin ligase cullin 7 induces epithelial−mesenchymal transition in human choriocarcinoma cells. *J Biol Chem* 2010;**285**:10870−9.
35. Lander R, Nordin K, LaBonne C. The F-box protein Ppa is a common regulator of core EMT factors Twist, Snail, Slug, and Sip1. *J Cell Biol* 2011;**194**:17−25.
36. Wang SP, Wang WL, Chang YL, Wu CT, Chao YC, Kao SH, et al. p53 controls cancer cell invasion by inducing the MDM2-mediated degradation of Slug. *Nat Cell Biol* 2009;**11**:694−704.
37. Wu ZQ, Li XY, Hu CY, Ford M, Kleer CG, Weiss SJ. Canonical Wnt signaling regulates Slug activity and links epithelial−mesenchymal transition with epigenetic breast cancer 1, early onset (BRCA1) repression. *Proc Natl Acad Sci U S A* 2012;**109**:16654−9.
38. Gu LB, Zhang HL, Liu T, Zhou S, Du YH, Xiong J, et al. Discovery of dual inhibitors of MDM2 and XIAP for cancer treatment. *Cancer Cell* 2016;**30**:623−36.
39. Du K, Herzig S, Kulkarni RN, Montminy M. TRB3: a tribbles homolog that inhibits Akt/PKB activation by insulin in liver. *Science* 2003;**300**:1574−7.
40. Hua F, Li K, Yu JJ, Lv XX, Yan J, Zhang XW, et al. TRB3 links insulin/IGF to tumour promotion by interacting with p62 and impeding autophagic/proteasomal degradations. *Nat Commun* 2015;**6**:7951.
41. Tomcik M, Palumbo-Zerr K, Zerr P, Sumova B, Avouac J, Dees C, et al. Tribbles homologue 3 stimulates canonical TGF-beta signalling to regulate fibroblast activation and tissue fibrosis. *Ann Rheum Dis* 2016;**75**:609−16.
42. Ravid T, Hochstrasser M. Diversity of degradation signals in the ubiquitin−proteasome system. *Nat Rev Mol Cell Biol* 2008;**9**:679−90.
43. Li K, Lv XX, Hua F, Lin H, Sun W, Cao WB, et al. Targeting acute myeloid leukemia with a proapoptotic peptide conjugated to a Toll-like receptor 2-mediated cell-penetrating peptide. *Int J Cancer* 2014;**134**:692−702.
44. Tanimura S, Ohtsuka S, Mitsui K, Shirouzu K, Yoshimura A, Ohtsubo M. MDM2 interacts with MDMX through their RING finger domains. *FEBS Lett* 1999;**447**:5−9.
45. Chen J, Marechal V, Levine AJ. Mapping of the p53 and mdm-2 interaction domains. *Mol Cell Biol* 1993;**13**:4107−14.
46. Yu JM, Sun W, Wang ZH, Liang X, Hua F, Li K, et al. TRIB3 supports breast cancer stemness by suppressing FOXO1 degradation and enhancing SOX2 transcription. *Nat Commun* 2019;**10**:5720.
47. Hua F, Mu R, Liu J, Xue J, Wang Z, Lin H, et al. TRB3 interacts with SMAD3 promoting tumor cell migration and invasion. *J Cell Sci* 2011;**124**:3235−46.
48. Walensky LD, Bird GH. Hydrocarbon-stapled peptides: principles, practice, and progress. *J Med Chem* 2014;**57**:6275−88.
49. Wynn TA. Integrating mechanisms of pulmonary fibrosis. *J Exp Med* 2011;**208**:1339−50.
50. Mora AL, Rojas M, Pardo A, Selman M. Emerging therapies for idiopathic pulmonary fibrosis, a progressive age-related disease. *Nat Rev Drug Discov* 2017;**16**:810.
51. Tang Y, Weiss SJ. Snail/Slug-YAP/TAZ complexes cooperatively regulate mesenchymal stem cell function and bone formation. *Cell Cycle* 2017;**16**:399−405.
52. Perez-Mancera PA, Gonzalez-Herrero I, Perez-Caro M, Gutierrez-Cianca N, Flores T, Gutierrez-Adan A, et al. SLUG in cancer development. *Oncogene* 2005;**24**:3073−82.
53. Yao C, Su L, Shan J, Zhu C, Liu L, Liu C, et al. IGF/STAT3/NANOG/Slug signaling axis simultaneously controls epithelial−mesenchymal transition and stemness maintenance in colorectal cancer. *Stem Cell* 2016;**34**:820−31.
54. Sun Y, Shao L, Bai H, Wang ZZ, Wu WS. Slug deficiency enhances self-renewal of hematopoietic stem cells during hematopoietic regeneration. *Blood* 2010;**115**:1709−17.
55. Liu Z, Wu H, Jiang K, Wang Y, Zhang W, Chu Q, et al. MAPK-mediated YAP activation controls mechanical-tension-induced pulmonary alveolar regeneration. *Cell Rep* 2016;**16**:1810−9.
56. Rock JR, Barkauskas CE, Cronce MJ, Xue Y, Harris JR, Liang JR, et al. Multiple stromal populations contribute to pulmonary fibrosis without evidence for epithelial to mesenchymal transition. *Proc Natl Acad Sci U S A* 2011;**108**:E1475−83.
57. Diaz VM, Vinas-Castells R, Garcia de Herreros A. Regulation of the protein stability of EMT transcription factors. *Cell Adhes Migrat* 2014;**8**:418−28.
58. Inoue Y, Itoh Y, Sato K, Kawasaki F, Sumita C, Tanaka T, et al. Regulation of epithelial−mesenchymal transition by E3 ubiquitin ligases and deubiquitinase in cancer. *Curr Cancer Drug Targets* 2016;**16**:110−8.
59. Skaar JR, Pagan JK, Pagano M. Mechanisms and function of substrate recruitment by F-box proteins. *Nat Rev Mol Cell Biol* 2013;**14**:369−81.
60. Kao SH, Wang WL, Chen CY, Chang YL, Wu YY, Wang YT, et al. GSK3beta controls epithelial−mesenchymal transition and tumor metastasis by CHIP-mediated degradation of Slug. *Oncogene* 2014;**33**:3172−82.
61. Hung PF, Hong TM, Chang CC, Hung CL, Hsu YL, Chang YL, et al. Hypoxia-induced Slug SUMOylation enhances lung cancer metastasis. *J Exp Clin Cancer Res* 2019;**38**:5.
62. Qi L, Heredia JE, Altarejos JY, Screaton R, Goebel N, Niessen S, et al. TRB3 links the E3 ubiquitin ligase COP1 to lipid metabolism. *Science* 2006;**312**:1763−6.
63. Salazar M, Lorente M, Garcia-Taboada E, Perez Gomez E, Davila D, Zuniga-Garcia P, et al. Loss of tribbles pseudokinase-3 promotes Akt-driven tumorigenesis *via* FOXO inactivation. *Cell Death Differ* 2015;**22**:131−44.
64. Zhang XW, Zhou JC, Peng D, Hua F, Li K, Yu JJ, et al. Disrupting the TRIB3−SQSTM1 interaction reduces liver fibrosis by restoring autophagy and suppressing exosome-mediated HSC activation. *Autophagy* 2020;**16**:782−96.
65. Liu SS, Lv XX, Wei XP, Liu C, Li Q, Min JL, et al. TRIB3−GSK-3β interaction promotes lung fibrosis and serves as a potential therapeutic target. *Acta Pharm Sin B* 2021;**11**:3105−19.
66. Varone F, Montemurro G, Macagno F, Calvello M, Conte E, Intini E, et al. Investigational drugs for idiopathic pulmonary fibrosis. *Expet Opin Invest Drugs* 2017;**26**:1019−31.
67. Moon H, Lim HS. Synthesis and screening of small-molecule alpha-helix mimetic libraries targeting protein-protein interactions. *Curr Opin Chem Biol* 2015;**24**:38−47.
68. Yang J, Velikoff M, Canalis E, Horowitz JC, Kim KK. Activated alveolar epithelial cells initiate fibrosis through autocrine and paracrine secretion of connective tissue growth factor. *Am J Physiol Lung Cell Mol Physiol* 2014;**306**:L786−96.
69. Lovisa S, LeBleu VS, Tampe B, Sugimoto H, Vadnagara K, Carstens JL, et al. Epithelial-to-mesenchymal transition induces cell cycle arrest and parenchymal damage in renal fibrosis. *Nat Med* 2015;**21**:998−1009.